Structures 71 (2025) 107857

Contents lists available at ScienceDirect

Structures

journal homepage: www.elsevier.com/locate/structures

Design strength parameters of dot-by-dot Wire-and-Arc Additively Manufactured stainless steel bars

Vittoria Laghi *, Lidiana Arrè, Giada Gasparini, Tomaso Trombetti, Michele Palermo

Department of Civil, Chemical, Environmental and Materials Engineering (DICAM) - University of Bologna, Viale del Risorgimento, Bologna 2-40136, Italy

ARTICLE INFO

Keywords:
Directed energy deposition
Wire-and-arc additive manufacturing
Stainless steel
Experimental tests
Design values
Partial safety factors
Confidence interval

ABSTRACT

Wire-and-Arc Additive Manufacturing (WAAM) is a promising solution to build a new generation of efficient steel structures with reduced material use. The dot-by-dot printing strategy enables to manufacture complex lattice steel structures such as diagrid elements and rebars for free-form reinforced concrete elements. Their structural application requires reliable design procedure for the full exploitation of WAAM in Architecture, Engineering and Construction (AEC) industry. The present study focuses on the calibration of design strength parameters of dot-by-dot WAAM-produced 304 L stainless steel straight bars based on the results of tensile tests performed on batches of specimens produced with different build angles (i.e. 0°, 10° and 45°). The results are then grouped into samples, the first three samples corresponding to the individual batches of specimens produced with the different build angles (i.e. 0°, 10° and 45°), to assess the influence of the printing inclination on the mechanical response, while the fourth sample merging the specimens produced at 0° and 10° to account for the effect of the sample size in a statistical way. The calibrated characteristic and ultimate limit state design values (both at yielding and ultimate conditions) and corresponding partial safety factors are evaluated according to the best-fit statistical distributions derived from the experimental test results. Two different approaches are compared to account for the effects of the sample size: one based on Eurocode 0 "design assisted by testing" procedure, and one based on the estimation of the confidence interval of both the 5 % and 0.1 % percentiles (corresponding to the characteristic and ultimate limit state design values). Additional considerations are also made on the strength hardening ratio. The results indicate that, for the investigated dot-by-dot WAAM process, a build angle higher than 10° could have significant effects on the design values and partial safety factors, therefore it should be properly accounted in the structural design stage.

1. Introduction

Metal Additive Manufacturing, particularly Wire Arc Additive Manufacturing (WAAM), has proved to be a promising technology for producing optimized steel structures that ensure efficiency by reducing material use and waste, while simultaneously minimizing safety risks on construction sites [1–3].

Extensive research effort has been paid on applications of WAAM for efficient structural steel systems. Among others, Ye et al. proposed an end-to-end framework to design and fabricate optimized tubular structures with WAAM [4]. An environmental life-cycle assessment of WAAM optimized parts has been performed in [5], confirming the improved environmental impact of WAAM-produced components if optimization techniques are employed. More recently, Laghi and Gasparini proposed an integrated design and fabrication approach to realize resource-efficient beams and lattice columns with WAAM technology [6]. The latter were produced with the so-called dot-by-dot (or point-by-point) printing strategy, adopted to fabricate single bars [7–9], grids for reinforcement of concrete structures [9] and lattice elements [10].

When dealing with WAAM elements several aspects should be carefully evaluated. The inherent surface roughness proper of the printing process could have a detrimental effect on the mechanical properties [8,11]. A marked mechanical anisotropy could manifest especially for stainless steel elements, as a consequence of the specific microstructure [12–14] influenced by the process parameters [15]. These considerations evidence the strong coupling effects of the specific geometrical features and mechanical properties, resulting from the printing strategy, on the structural behavior of WAAM systems. One possibility to account for these issues directly is to follow a "design by advanced analysis" approach, resulting in a complex non-linear finite

* Corresponding author.
E-mail address: vittoria.laghi2@unibo.it (V. Laghi).

https://doi.org/10.1016/j.istruc.2024.107857
Received 22 February 2024; Received in revised form 23 October 2024; Accepted 15 November 2024

Nomenclature

The following symbols are used in this paper

A(z)	real cross-sectional area
A_{eff}	effective cross-sectional area
A_{min}	minimum cross-sectional area
A_n	nominal cross-sectional area
CI	Confidence Interval
CL	Confidence Level
CL-G	Confidence Level of the best-fit Gaussian statistical distribution
CL-LN	Confidence Level of the best-fit Log-Normal statistical distribution
COV	coefficient of variation
COV_{exp}	coefficient of variation of the experimental statistical distribution
COV_G	coefficient of variation of the best-fit Gaussian statistical distribution
COV_L	coefficient of variation of the best-fit Log-Normal statistical distribution
COV_W	coefficient of variation of the best-fit Weibull statistical distribution
E	Young's modulus
EC0-K	EC0 approach in case of known coefficient of variation
EC0-UK	EC0 approach in case of unknown coefficient of variation
KS_G	Kolmogorov-Smirnov test for the best-fit Gaussian statistical distribution
KS_L	Kolmogorov-Smirnov test for the best-fit Log-Normal statistical distribution
KS_W	Kolmogorov-Smirnov test for the best-fit Weibull statistical distribution
R_0	proportionality tensile resistance
R_u	ultimate tensile resistance
R_y	yield tensile resistance
X	strength random variable
b-a	build angle
dot-0, dot-10, dot-45	specimens printed at 0°, 10° and 45° build angles, respectively
$d_{real}(z)$	real value of bar diameter
f_0	material proportionality strength corresponding to 0.01 % proof stress
$f_{0,eff}$	effective material proportionality strength corresponding to 0.01 % proof stress
$f_{0,n}$	nominal material proportionality strength corresponding to 0.01 % proof stress
f_y	yield tensile strength corresponding to 0.2 % proof stress
$f_{y,d\text{-}CL}$	Ultimate Limit State design value of the yield tensile strength estimated according to the Confidence Level approach
$f_{y,d\text{-}EC0}$	Ultimate Limit State design value of the yield tensile strength estimated according to EC0 approach
$f_{y,eff}$	effective yield tensile strength corresponding to 0.2 % proof stress
$f_{y,k\text{-}CL}$	characteristic design value of the yield tensile strength estimated according to the Confidence Level approach
$f_{y,k\text{-}EC0}$	characteristic design value of the yield tensile strength estimated according to EC0 approach
$f_{y,n}$	nominal yield tensile strength corresponding to 0.2 % proof stress
f_u	ultimate tensile strength
$f_{u,d\text{-}CL}$	Ultimate Limit State design value of the ultimate tensile strength estimated according to the Confidence Level approach
$f_{u,k\text{-}CL}$	characteristic design value of the ultimate tensile strength estimated according to the Confidence Level approach
$f_{u,k\text{-}EC0}$	characteristic design value of the ultimate tensile strength estimated according to EC0 approach
$f_{u,d\text{-}EC0}$	Ultimate Limit State design value of the ultimate tensile strength estimated according to EC0 approach
$f_{u,eff}$	effective ultimate tensile strength
$f_{u,n}$	nominal ultimate tensile strength
h	sample size
k	fractile / tolerance factor
$k_{d,n}$	fractile factor for the Ultimate Limit State design value
k_n	fractile factor for the characteristic design value
L	bar length
m	mean value
m_{exp}	mean value of the experimental statistical distribution
m_G	mean value of the best-fit Gaussian distribution
m_L	mean value of the best-fit Lognormal distribution
m_W	mean value of the best-fit Weibull distribution
m_y	mean value of the best-fit Lognormal statistical distribution associated with the sample
n-a	nozzle angle
p	probability
s	standard deviation
s_{exp}	standard deviation of the experimental statistical distribution
s_G	standard deviation of the best-fit Gaussian statistical distribution
s_L	standard deviation of the best-fit Lognormal statistical distribution
s_W	standard deviation of the best-fit Weibull statistical distribution
s_y	standard deviation of the best-fit Lognormal statistical distributione associated with the sample
t	percentile of the noncentral t-distribution
$\widehat{x_{0.1\%-G}}$	0.1 % percentile of the best-fit Gaussian statistical distribution
$\widehat{x_{0.1\%-LN}}$	0.1 % percentile of the best-fit Log-Normal statistical distribution
$\widehat{x_{5\%-G}}$	5 % percentile of the best-fit Gaussian statistical distribution
$\widehat{x_{5\%-LN}}$	5 % percentile of the best-fit Log-Normal statistical distribution
$x_{d\text{-}EC0}$	Ultimate Limit State design value of the strength according to EC0 approach
$x_{k\text{-}EC0}$	characteristic design value of the strength according to EC0 approach
$\widehat{x_{p-G}}$	p-percentile of the best-fit Gaussian statistical distribution
$\widehat{x_{p-LN}}$	p-percentile of the best-fit Log-Normal statistical distribution
z(p)	CDF value of the standard normal Gaussian distribution corresponding to p
ΔL	portion of bar length
$\gamma_{0v\text{-}CL}$	material overstrength factor estimated according to the Confidence Level approach
$\gamma_{0v\text{-}EC0}$	material overstrength factor estimated according to EC0 approach
$\gamma_{M\text{-}CL}$	partial safety factor estimated according to the Confidence Level approach
$\gamma_{M\text{-}EC0}$	partial safety factor estimated according to EC0 approach
γ_{M0}	partial safety factor for material strength according to Eurocode
γ_{M2}	partial safety factor for ultimate strength according to Eurocode
δ	non-centrality parameter of the non-central t-distribution
$\eta_{d\text{-}CL}$	strength hardening ratio of Ultimate Limit State design values estimated according to the Confidence Level

	approach
$\eta_{d\text{-}EC0}$	strength hardening ratio of Ultimate Limit State design values estimated according to EC0 approach
$\eta_{k\text{-}CL}$	strength hardening ratio of the characteristic design values estimated according to the Confidence Level approach
$\eta_{k\text{-}EC0}$	strength hardening ratio of the characteristic design values estimated according to EC0 approach
σ_{eff}	axial stress evaluated considering the effective cross-sectional area
$\sigma_{(n)}$	axial stress evaluated considering the nominal cross-sectional area
$\sigma_{(z)}$	axial stress evaluated considering the real cross-sectional area

element model of the structure [16] as recently proposed by Gardner et al. [17]. Nevertheless, such advanced simulation tools require high computational skills beyond the capabilities of professional structural engineers [18]. An alternative approach is based on the use of conventional design procedures based on equivalent linear elastic models using appropriate design values and partial safety factors, according to the "design assisted by testing" provisions in Annex D of Eurocode 0 (EC0) (EN 1990) [19]. The latter allows to calibrate the design strength parameters and partial safety factors of new construction materials through statistical analysis of the experimental results, even in presence of a limited sample size (number of specimens $n < 10$), using the so-called tolerance factor (k) for the estimation of the characteristic and Ultimate Limit State (ULS) design values. This approach was also adopted to calibrate design values and partial safety factors of various steel members and components subjected to complex loading conditions (see e.g. [20–22]). The values adopted in EC0 were calibrated using a Bayesian approach that would correspond to a statistical estimation at a 75 % confidence level. In the work by Monti and Petrone [23], a Bayesian method was proposed to calibrate the value of partial safety factors for capacity models based on the estimation of tolerance factors at any confidence level. The proposed formulation assumed a normal distribution for the resistance model. The EC0 approach has been recently adopted by the authors to evaluate, for the first time, design values and corresponding partial safety factors of 304L stainless steel parts obtained through layer-by-layer WAAM deposition process with a constant set of printing parameters. For this aim, the results of tensile tests on dog-bone specimens, extracted from stainless steel plates along different directions, were analyzed, thus accounting for their inherent anisotropy [24]. Clearly, the quantitative results are only suitable for the investigated alloy and set of WAAM process. A similar approach has been adopted by Arrayago et al. and Meza et al., who focused on calibrating material factors for stainless steel, considering a large dataset collected from literature and producers [25,26]. In particular, Arrayago et al. [25] examined the key sources of uncertainty to be considered in the design of stainless steel structures, providing statistical functions and probabilistic models for the main random variables (e.g. geometric properties, material parameters and imperfections) that influence the strength of stainless steel structures.

The present study aims at evaluating the characteristic and Ultimate Limit States (ULS) design values and corresponding partial safety factors of dot-by-dot WAAM-produced 304 L stainless steel bars printed at different orientations with a constant set of printing parameters. The design values and partial safety factors are evaluated by interpreting the results of tensile tests carried out on three production batches, considering three different build angles (i.e. 0°, 10° and 45°) of the printed bars. First, a statistical analysis is carried out considering both the nominal stress obtained from the nominal cross-sectional area and the effective stress associated with the effective cross-sectional area obtained from volume equivalency, originally proposed by [27] and then employed by [11,28,29]. Correlation studies are then performed on the geometrical and mechanical quantities (i.e. cross-sectional area vs tensile resistance). The results of the statistical analysis are further interpreted to calibrate the characteristic and ULS design values and corresponding partial safety factors, as well as material overstrength and strength hardening ratio. The standard EC0 "design assisted by testing" approach is compared with an alternative approach based on a general statistical analysis aimed at estimating the characteristic and ULS design values at a given Confidence Level (CL) based on the percentile Confidence Interval (CI) [30,31]. Both approaches (EC0 and CL) are capable of explicitly dealing with a sample of limited size. The comparison of the results of the two approaches represents a novel aspect of the present work and opens further investigations toward the definition of specific structural design guidelines for WAAM-produced structures. Finally, additional discussions and considerations are also made on the overstrength factor and strength hardening ratio.

2. Tensile behavior of dot-by-dot WAAM stainless steel bars

2.1. The experimental investigation on dot-by-dot WAAM bars

An extensive experimental investigation has been carried out at University of Bologna to assess the geometrical, microstructural and mechanical features of dot-by-dot WAAM-produced stainless steel bars.

The first experimental campaign was carried out on a production of 29 WAAM-produced stainless steel single bars. The bars were first 3D scanned to characterize their geometrical features, then tested when subjected to tensile loading, considering 3 different build angles (b-a) at 0°, 10° and 45°, keeping a fixed nozzle angle (n-a) of 0°. The build angle refers to the angle between the longitudinal axis of the WAAM bar and the vertical axis (perpendicular to the base platform), while the nozzle angle indicates the angle between the axis of the WAAM bar (z-axis) and the nozzle axis, as shown in Fig. 3. The specimens printed with different build angles will be also referred to as dot- 0 specimens, dot-10 specimens and dot-45 specimens. The bars tested under tensile loading were also analyses in terms of their microstructural features through metallographic analyses, based on the use of optical and scanning electron microscopy. Further details can be found in [29].

A second experimental campaign was carried out on a batch of 10 WAAM-produced single bars considering a fixed build angle of 0°. The bars were 3D scanned to characterize their geometrical features, then tested first under bending loading (three-point bending set-up) within the elastic range, and then in compression. The results of the geometrical characterization and three-point bending tests were presented in [32], while the results of the compression tests were presented in [33]. This work will focus on the interpretation of the results of tensile tests from the first experimental campaign.

2.2. Dot-by-dot WAAM process

The bars were fabricated by the Dutch company MX3D [34] adopting the so-called dot-by-dot printing strategy. It consists of the successive deposition of metal droplets along the longitudinal axis of the bar (see Fig. 1) resulting in a nominal diameter directly related to the drop of liquid metal, with one main growing direction. All bars were manufactured using the same set of process parameters to allow meaningful comparison of the different production batches. It is worth noticing that the process parameters were not specifically optimized to achieve selected mechanical performances of the bar, rather they represented the know-how of the manufacturer at the time of the production.

In detail, the welding source used was Gas Metal Arc Welding

(GMAW) with the process parameters lying within the following ranges: current of 100–140 A, arc voltage of 18–21 V, welding speed of 15–30 mm/s, wire feed rate of 4–8 m/min and deposition rate of 0.5–2 kg/h. It should be noted that the values of the process parameters provided above are reported with their typical ranges as given by the manufacturer, while for more specific information the interested reader could refer directly to the manufacturer [34]. The average layer height was set to 1 mm. A commercially available standard stainless steel welding wire grade ER308LSi (1 mm diameter) supplied by Oerlikon [35] was used. The used substrate was a printing plate of 1000 × 1000×30 mm, with H-type beams welded as support.

The nominal diameter of the bar is influenced by both the wire diameter and the printing parameters that affect the size of the liquid metal droplet. The printing process parameters adopted by MX3D led to a nominal diameter of 6 mm. However, the real cross-sectional shape of the bar is irregular, changing while moving along the z-axis. As an initial approximation, the cross-section can be modelled as a circular shape of diameter $d_{real}\ (z)$ continuously changing with z. In particular, when metal droplets are deposited sequentially, the real diameter of the cross-section varies along the z-axis of the bar, approximately around 0.5 mm [29]. This variation results in a noticeable surface roughness, similar to the surface irregularities generated by the layer-by-layer deposition in continuously printed plates [36]. Moreover, the successive deposition can introduce deviations from a straight path, resulting in some lack of straightness due to imprecise torch positioning, which affects the geometrical precision of the printed elements. Consequently, the dot-by-dot deposition leads to a non-uniform circular cross-section and non-straight longitudinal axis (defined by the polyline connecting the centroids of each circular cross-section along the bar). Therefore, it becomes evident that the internal axial stress $\sigma(z)$ of a WAAM bar subjected to an external tensile axial force will exhibit continuous variations along the z-axis, as qualitatively shown in Fig. 2.

2.3. Interpretation of the mechanical behavior of dot-by-dot WAAM bars subjected to tensile loading

From a mechanical point of view, at first approximation as an alternative to the continuum mechanics approach, the tensile behavior of dot-by-dot WAAM bars could be described by a system of i non-linear axial springs connected in series, as shown in Fig. 2. Each spring represents a small portion of the bar of length ΔL, characterized by the following properties:

- a material stress-strain constitutive law described by the two-stage Ramberg-Osgood (RO) model [37], then extended by Rasmussen [38], as represented in Fig. 2. The symbols have the following meanings: E indicates the material Young's modulus; f_0, f_y and f_u, indicate the material proportionality tensile strength (typically assumed equal to the 0.01 % proof stress), the yield tensile strength (typically assumed equal to the 0.2 % proof stress) and the ultimate tensile strength, respectively; the material properties are assumed constant along the whole bar.
- an average cross-sectional area equal to A_i;
- an average axial stiffness equal to $EA_i/\Delta L$;
- key resistance values corresponding to: proportionality tensile resistance $R_{0,i}=A_i f_0$, yield tensile resistance $R_{y,i}=A_i f_y$, and ultimate tensile resistance $R_{u,i}=A_i f_u$.

Since the material strength parameters f_0, f_y and f_u are assumed constant along the whole bar length, the proportionality resistance (R_0), the yield resistance (R_y) and ultimate resistance (R_u) of the entire bar will correspond to the axial force value leading to the proportional, yield and ultimate tensile strengths, respectively, of the spring associated to the portion of minimum area, e.g. $A_i = A_{min}$. The three resistance values allow to identify the three key response points denoted as P_0, P_y and P_u in the force-elongation graph of Fig. 2.

The mechanical analogy introduced above facilitates the interpretation of the force-elongation response of the stainless steel WAAM bar in tension as qualitatively illustrated in Fig. 2, which is typically characterized by a low proportionality limit followed by yielding and a significant hardening behavior up to the final failure (see e.g. [29]). It is thus clear that the smooth nature of the force-elongation response of the whole WAAM bar depends on the coupling of the inherent smooth nature of stainless steel stress-strain behavior with the geometrical irregularities proper of WAAM bars.

The evaluation of the full axial stress state would require complete knowledge of the exact geometry of the bar (Fig. 2). However, in a structural design process, the detailed geometrical description of each bar is not available. For that, alternative design approaches based on an equivalent uniform bar model considering either nominal or effective values of cross-sectional area could be employed (Fig. 1).

For this reason, the authors proposed three approaches to model the geometrical and mechanical parameters of WAAM-produced bars:

- Approach 1: a nominal equivalent geometry is considered, having constant diameter along the length of the bar corresponding to the digital input of the printing process. Hereafter this approach is referred also as "nominal" approach. The use of the nominal cross-sectional area A_n leads to the evaluation of nominal material strength values associated with the proportionality, yield and ultimate tensile resistances as follows:

$$f_{0,n} = R_0 \Big/ A_n \tag{1}$$

$$f_{y,n} = R_y \Big/ A_n \tag{2}$$

$$f_{u,n} = R_u \Big/ A_n \tag{3}$$

- Approach 2: a volume-equivalent geometry is considered, having constant diameter along the length of the bar corresponding to the diameter of the volume-equivalent uniform bar. This value is taken from volume measures following the Archimedes' principle, see e.g. [29]. Hereafter this approach is referred also as "effective" approach. The use of the effective cross-sectional area leads to the evaluation of effective strength values associated with the proportionality, yield and ultimate tensile resistances as follows:

$$f_{0,eff} = R_0 \Big/ A_{eff} \tag{4}$$

$$f_{y,eff} = R_y \Big/ A_{eff} \tag{5}$$

$$f_{u,eff} = R_u \Big/ A_{eff} \tag{6}$$

- Approach 3: the real geometry is considered, having a variable diameter along the length of the bar. This value can be taken from 3D scan acquisition measures, see e.g. [11,29,32]. Hereafter this approach is referred also as "real" approach. In this case the material strength values associated to the proportionality, yield and ultimate tensile resistances can be evaluated considering the minimum cross-sectional area as follows:

$$f_0 = R_0 / A_{\min} \tag{7}$$

$$f_y = R_y \Big/ A_{\min} \tag{8}$$

$$f_u = R_u / A_{\min} \tag{9}$$

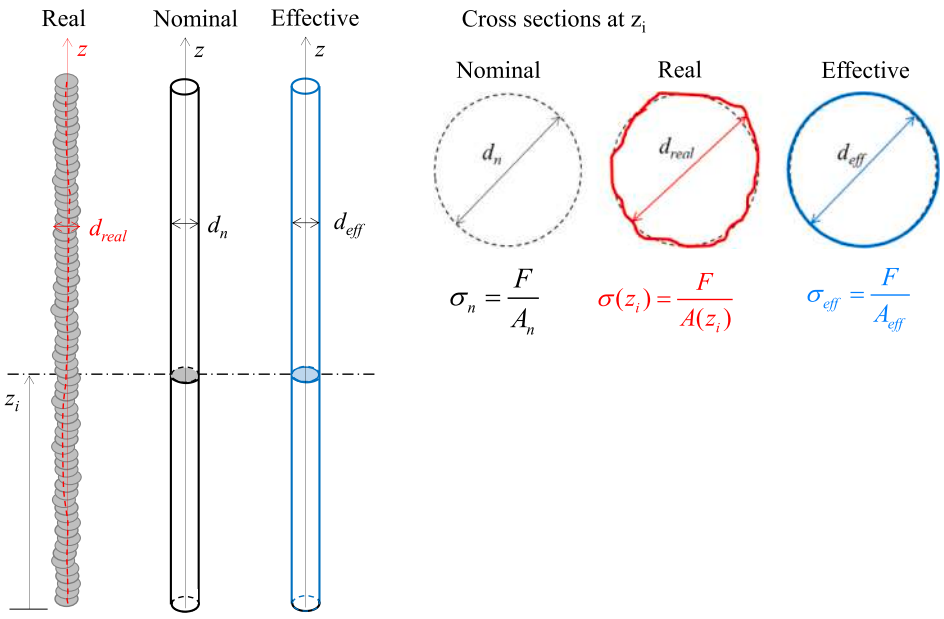

Fig. 1. Geometrical models of a straight dot-by-dot WAAM bar and related axial stress under tension.

In Section 3 a statistical analysis on the variability and correlation between the single design resistance variables, namely the proportionality, yield and ultimate resistance values (R_0, R_y and R_u) and the effective area (A_{eff}), is carried out considering the results of previous tensile tests reported in [29] and briefly described hereafter.

2.4. The key geometrical and mechanical parameters investigated in the present work

The first production of dot-by-dot WAAM bars were tested under tensile loading, as explained in Section 2.1, to assess the influence of the build angle on the overall mechanical response of the printed bars, given the constant set of process parameters of the manufacturing company. In detail, 10 specimens were printed with build angles equal to 0° (dot-0 batch), and 10° (dot-10 batch) while 9 specimens were printed with a build angle of 45° (dot-45 batch) (Fig. 3). The case of 0° and 45° build angles corresponds to the common limit conditions of inclined printed bars for practical applications. The case of 10° build angle corresponds, instead, to a commonly adopted value for lattice structural elements (see e.g. [10]).

Considering the irregular cross-sectional shape and the lack of straightness of the longitudinal axis described in Section 2.2, the geometrical characterization involved the following steps: (i) analysis of

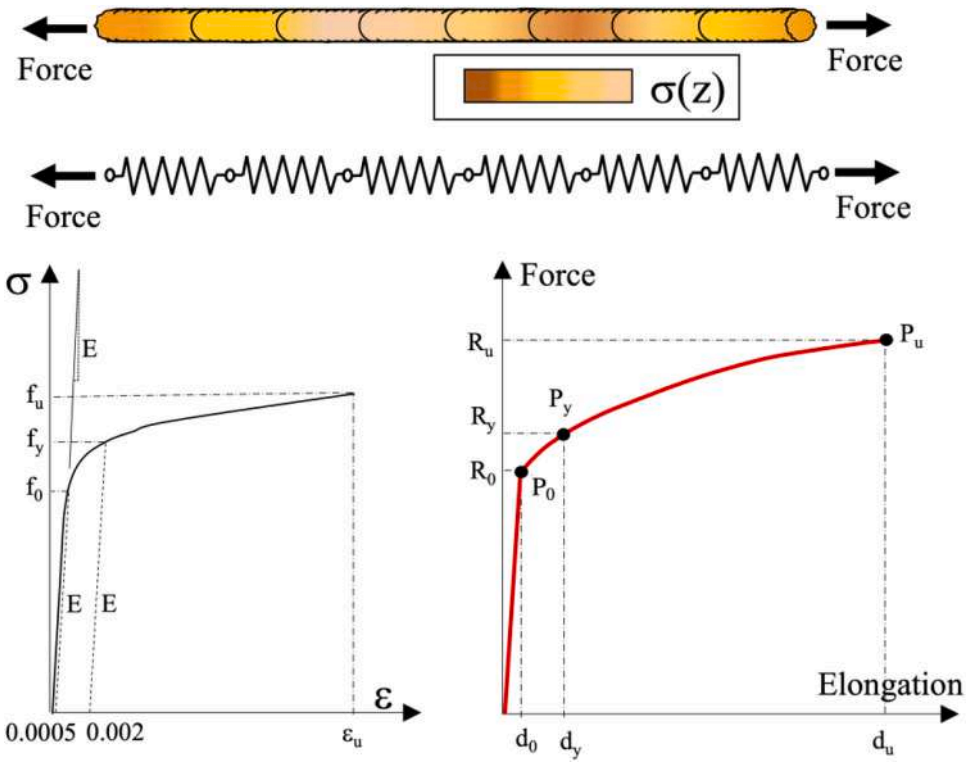

Fig. 2. Dot-by-dot WAAM stainless steel bar under tension: real axial stress field σ(z), mechanical analogy; material stress-strain behavior; force-elongation behavior of the whole bar.

the real cross-sectional area for each section along the longitudinal axis; (ii) evaluation of the real longitudinal axis (represented as a polyline which connects the real centroids of the cross-sections); (iii) assessment of the equivalent cross-sectional volume (for the purpose of determining effective stresses). The detailed results of the geometrical characterization are available in [29].

The mechanical characterization was performed through tensile tests on three batches of specimens, each one corresponding to a different build angle, for a total of 29 specimens tested.

The full description of the test set-up and the presentation of all test results can be found in [29]. The key mechanical parameters were originally evaluated in terms of effective properties considering the effective cross-sectional area (see e.g. [11,28]), according to the procedure commonly adopted to characterize the behavior of stainless steel material (see e.g. [37,39]).

Among all the results obtained from the tensile tests, the following key geometrical and mechanical parameters are investigated more in depth in the present work: (i) the effective cross-sectional area (A_{eff}), (ii) the yield and ultimate tensile resistances, namely R_y and R_u respectively, and strengths, namely f_y and f_u, respectively. The yield strength values are calculated from the 0.2 % proof stress values.

Fig. 4 summarizes the experimental results obtained for the three batches in terms of the main parameters investigated, namely effective areas and key resistance parameters.

The results on the effective cross-sectional area show that, on average, for small build angles (i.e. dot-0 and dot-10) the specimens present lower effective values with respect to the nominal one (corresponding to a nominal diameter equal to 6 mm). On the contrary, dot-45 specimens present, on average, higher effective values with respect to the nominal one. This finding was attributed to the increasing geometrical irregularities resulting from the higher build angle [29], as also observed in [8]. For all three build angles the COV values were around 10 % (see details in Section 3.1).

Some first considerations can be made regarding the yield and ultimate tensile resistances (R_y and R_u) and strengths (f_y and f_u). The mean values of both R_y and R_u are similar when considering dot-0 and dot-10 specimens, while they decrease for the dot-45 specimens. Reasoning on the observed trends were attributed to the increasing geometrical irregularities resulting from the higher build angle coupled with the unfavorable orientation of the layer boundaries, with respect to the plane of maximum shear stress, observed when analyzing the surfaces of fracture [8,29]. Yield strength values f_y are slightly higher when compared with the ranges of values provided by building codes for conventionally manufactured 304L stainless steel. The opposite trend is, instead, observed for the ultimate strength f_u, whose mean values are smaller with respect to the conventional ones. Both yield and ultimate strength values do not seem to be much affected by the variability in the effective areas. In particular, for the dot-10 specimens, the ultimate strength values exhibit very small variability (COV=3 %). This aspect will be investigated more in detail in Section 3 and 5.

Table 1 quantifies the relative ratios between key geometrical and mechanical parameters of dot-by-dot WAAM stainless steel bars, in terms of: (i) effective to nominal cross-sectional area ratios A_{eff}/A_n, and (ii) ultimate to yield resistance ratios R_u/R_y (corresponding also to the stress ratio $\sigma_u/\sigma_{0.2}$ according to the RO constitutive model [37,38]). Additionally, the hardening exponents n and m (estimated according to [37] and [38] respectively) are provided. For small build angles (i.e. dot-0 and dot-10) the values of A_{eff}/A_n are, on average, slightly smaller than 1 (around 0.95), thus indicating a small discrepancy between effective and nominal cross-sectional areas. On the other hand, for higher build angles (i.e. dot-45) the discrepancy between the values of effective and nominal cross-sectional area increases, resulting in an average value of A_{eff}/A_n equal to 1.16.

The values of resistance ratios R_u/R_y are close to 2.0 for all the three build angles, thus indicating that the tested dot-by-dot WAAM stainless steel bars exhibit significantly larger hardening behavior than conventional stainless steel. This result has direct implications on the values of the strength hardening ratio to be suggested for design purposes, as investigated more in depth in Section 5.

2.5. Objective of the work

The main objective of the present work is to provide an insight into the results of the tensile tests with the aim of calibrating the main material strength-related parameters for structural design, such as the material partial safety factors, the material overstrength factors and the strength hardening ratios. These factors are of paramount importance especially when dealing with capacity design requirements related to seismic design issues.

Overall, the results of the tensile tests indicated that the dot-0 and dot-10 batches showed, on average, similar mechanical performances, while the dot-45 batch showed, on average, decreased performances. Therefore, for the sake of interpreting the results in a statistical sense, the specimens can be grouped in four different samples: the first three samples coincident with the single production batches, while the fourth sample can be obtained by merging the dot-0 and dot-10 samples in order to obtain a new sample of double size with respect to the size of the single batches.

The three individual batches will be considered in the first statistical study presented in Section 3 with the aim of evaluating the best fit distributions of the resistances and their correlation with the effective areas. Then, the four samples will be analyzed more in depth in Section 4 to assess the yield and ultimate tensile strength design values and the related material partial safety factors. Finally, a focus on the material overstrength factors and strength hardening ratios will be provided. The different strength parameters and related factors will be assessed comparing the statistical approach provided by EC0 using the tabulated tolerance factors with the statistical approach based on the estimation of the percentile of the experimental distributions with a given confidence level. Beside the specific results in terms of design values and related material factors, the comparison between the two approaches represent a novel contribution of the present work.

3. Statistical analysis of the main investigated variables

Before proceeding with the evaluation of the design values for yield and ultimate tensile strengths, and calibration of the corresponding partial safety factors, this section presents the main results of a statistical analysis on the design variables here considered (A_{eff}, R_y and R_u). The analysis was performed considering the three batches individually (dot-0, dot-10, dot-45).

3.1. Statistical and best-fit distributions

First, the experimental (based on statistical inference) and best-fit Gaussian (G), Lognormal (L), Weibull (W) cumulative distribution functions (CDF) of the design variables were computed using the "fitdist" command in Matlab for the three individual batches, e.g. dot-0, dot-10 and dot-45. The three selected probability function models are typically considered to assess the variability of the resistance parameters of both carbon and stainless structural steel [25,40].

The plots of the CDFs are provided in Figure A1 in Annex 1, while their mean values (m), standard deviations (s) and coefficients of variations (COV) are summarized in Table 2.

First, it can be noted that for all three variables the shapes of the Gaussian and Lognormal statistical distributions are close to each other, thus indicating close to symmetrical experimental distributions. Moreover, in general, the resistance distributions exhibited by dot-0 and dot-10 batches have comparable features in terms of mean values and COV, while the resistance distribution obtained from the dot-45 batch shows a smaller mean value coupled with a larger COV. Clearly, these features have a significant impact on the calibrated design values and partial

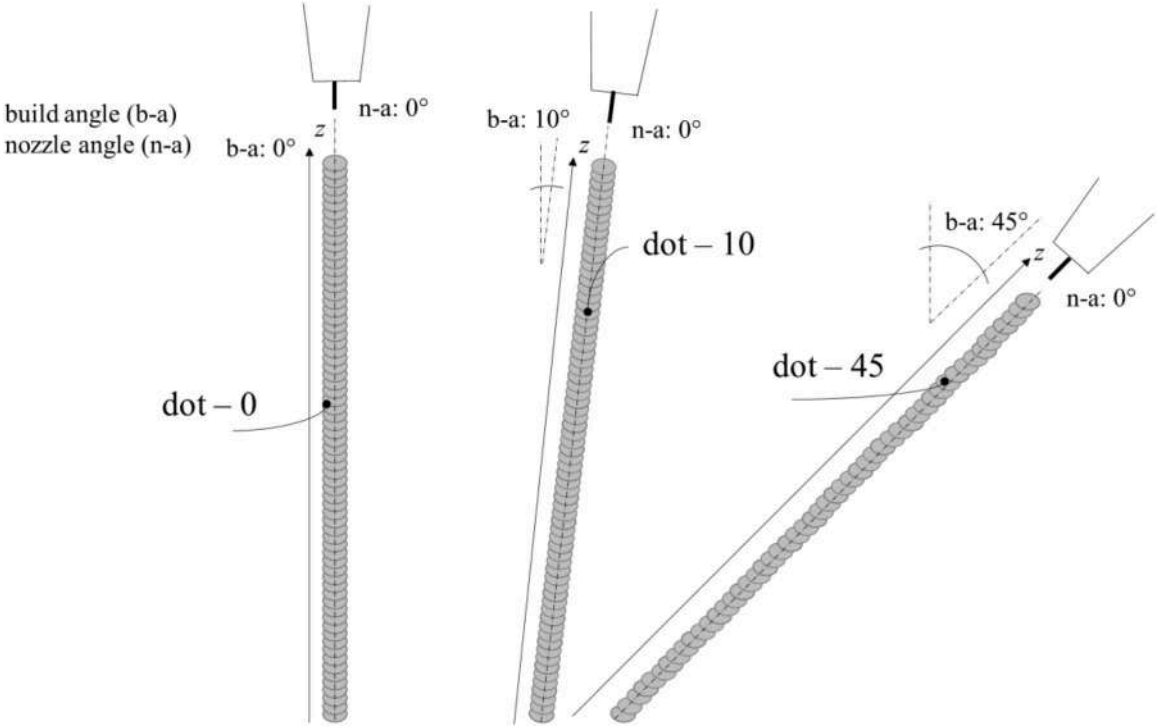

Fig. 3. Graphical representation of the WAAM bars printed with three different b-a: 0° (dot-0), 10° (dot-10) and 45° (dot-45). Adapted from [29].

safety factors, as illustrated in Section 5. Considering the variability of the results for each batch, the COV values of the effective cross-sectional area are between 6 % and 12 %, while yield and ultimate resistances have smaller variability (COV values of around 2–9 %). It is worth noticing, as already observed in Section 2.4, that the dot-10 batch evidenced a particularly small COV value (3 %) for the ultimate strength.

The goodness of fit of the three selected probability models is evaluated through the Kolmogorov-Smirnov test (in terms of KS coefficient [41] of the best-fit distributions evaluated from maximum likelihood estimators for the experimental data, whose the critical value for $\alpha = 0.05$ is 0.409) and Akaike information criterion (in terms of the modified AIC value for small sample size [42]) (Table 3). Overall, all the KS values are smaller than the critical one, thus indicating that the three distributions are a good fit for the experimental data. Moreover, among the three distributions (i.e. Gaussian, G, Weibull, W, Lognormal, L), as expected, the Lognormal and the Weibull distributions provide, in general, slightly smaller KS coefficients and larger AIC values, as compared with the ones of the Normal distribution. Finally, the goodness of the distributions was also assessed by visual diagnosis of the probability plots and the comparison of the empirical cumulative distribution functions (CDF) against the modelled ones.

Thus, in Section 5 both the Lognormal and Normal distributions will be considered to calibrate the design strength values of dot-by-dot WAAM stainless steel bars according to the Eurocode 0 approach presented in Section 4.1 (for the Lognormal distribution) and the design values following the approach introduced in Section 4.2 (for the Normal distribution).

3.2. Correlation analysis between effective area and resistance parameters

A correlation analysis was carried out to evluate the correlation between the effective area and both yield and ultimate tensile resistances.

First, the linear correlation coefficient between the resistance parameters (proportionality resistance, yield resistance and ultimate resistance) and the effective cross-sectional area was evaluated. The results are represented through the correlograms reported in Figure A2 of Annex 1. The plots evidence that, within the investigated narrow ranges of variation of the effective areas (around +/- 10 % of the nominal value), the yield and ultimate resistance are practically uncorrelated with the area. More in detail, Figure A2 in Annex 1 shows that: (i) the yield resistance is weakly positively correlated with the effective area (R^2 values between 0.017 and 0.269), (iii) the ultimate resistance has a weak negative correlation with the effective area (R^2 values between 0.072–0.327). The absence of a significant correlation between area and resistance values was then confirmed by computing the Kendall's tau and Spearman correlation coefficients which are capable of identifying a general monotonic correlation between two variables. For the sake of conciseness, those results are not reported here.

Hence, the absence of a significant correlation between effective area and both yield and ultimate resistances suggests that the effort required by the measurement of the effective cross-sectional area would not result in a more precise assessment of the resistance, concerning an estimation based on the sole knowledge of the nominal area. Therefore, for design purposes, using the nominal cross-sectional area would result in a level of reliability comparable to a design using the effective area, whose implementation would, however, require additional complexity. Consequently, the additional effort required to evaluate the effective cross-sectional areas of WAAM bars may not be justified by a significant benefit in terms of design strength prediction.

4. Calibration of the design values and partial safety factors

In this section two different approaches are implemented and compared to calibrate the characteristic and ULS design values for the two considered strength parameters, namely the yield strength and ultimate tensile strength, considering the four different samples previously described (i.e. the first three ones corresponding to the individual dot-0, dot-10 and dot-45 batches, while the fourth one corresponding to the merging of dot-0 and dot-10 batches). The results of the calibration analysis are then used to evaluate the material partial safety factors, the

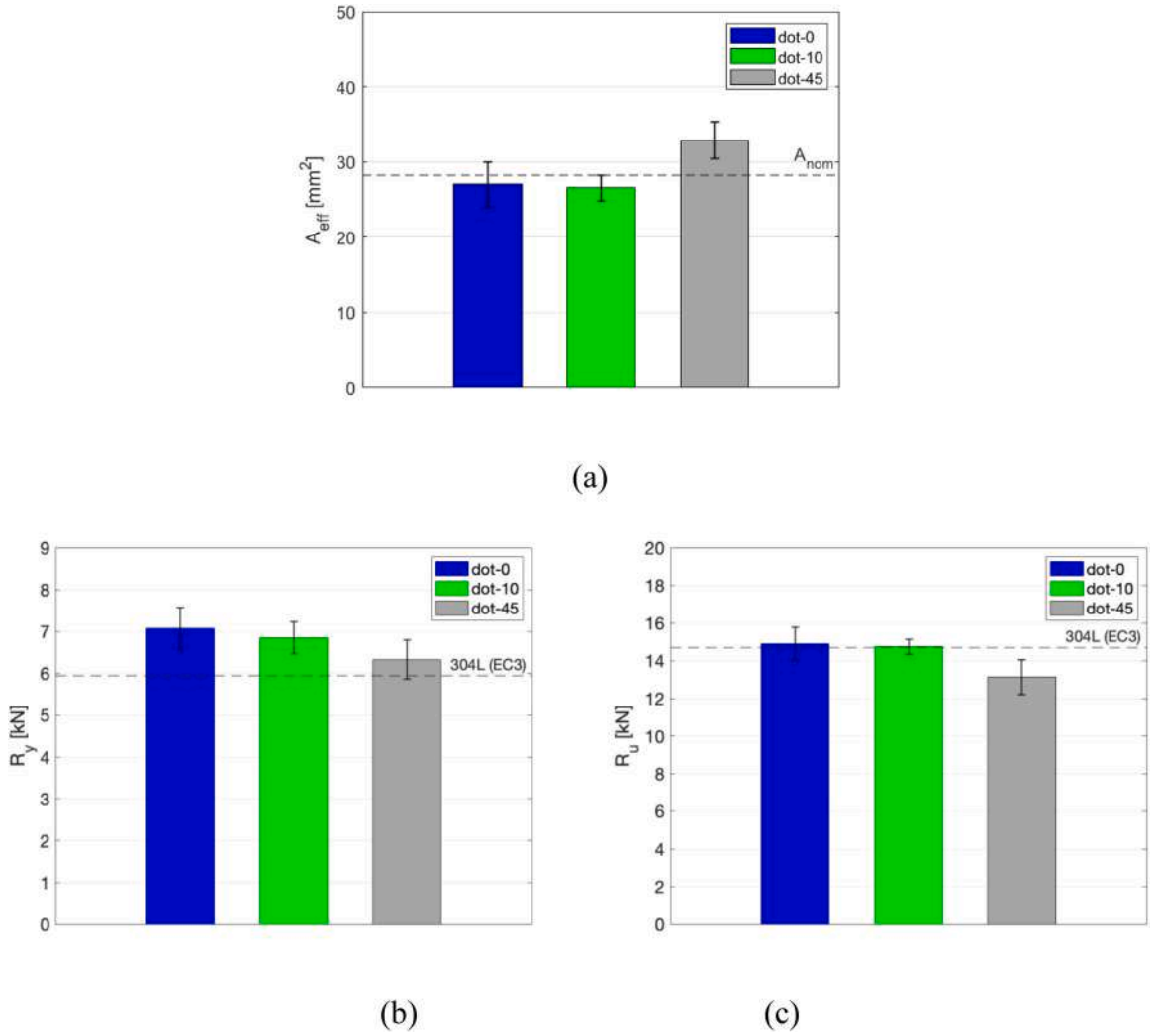

Fig. 4. Overview of the main experimental results considered in the present work in terms of bar charts representing mean values and standard deviations for the three different printing directions: (a) effective area; (b) yield tensile resistance; (c) ultimate tensile resistance.

Table 1
Key geometrical and mechanical parameters of dot-by-dot WAAM stainless steel bars.

Build angle		A_{eff}/A_n [-]	R_u/R_y [-]
0°	mean	0.97	2.09
	COV	10 %	6 %
10°	mean	0.95	2.14
	COV	5 %	5 %
45°	mean	1.16	2.09
	COV	8 %	12 %

material overstrength factors and the strength hardening ratios.

The first approach is the one provided by the Annex D of Eurocode 0 (EC0) [19], called "Design assisted by testing". The EC0 based approach was also initially employed for WAAM stainless steel planar elements in a previous work (see e.g. [24]). The second approach is based on estimating the design values at a given Confidence Level (CL) through the evaluation of the two-sided confidence interval (CI) of the selected percentiles, namely the 5 % percentile for the characteristic value and the 0.1 % percentile for the ULS design value. Both approaches explicitly account for the limited size of the samples.

It is worth noticing that, since the effective cross-sectional area showed very weak correlation with the resistance parameters, the nominal stress values, as computed using the nominal cross-sectional area according to Eqs. (1)–(3), are here considered to compute the values of the yield and ultimate tensile strengths starting from the corresponding resistance values.

4.1. EC0 Approach

The calibration of characteristic and ULS design values based on EC0 follows the "design assisted by testing" procedure reported in Annex D of EC0 [19]. The approach is applicable if the experimental distribution can be sufficiently well described by a Lognormal distribution. According to this approach, the characteristic (x_{k-EC0}) and ULS (x_{d-EC0}) design values of the strength parameter can be estimated using the following expressions:

$$x_{k-EC0} = \exp(m_y - k_n \cdot s_y) \tag{10}$$

$$x_{d-EC0} = \exp(m_y - k_{d,n} \cdot s_y) \tag{11}$$

where m_y and s_y are the mean value and standard deviation of the best-fit Lognormal distribution associated with the sample, respectively, while k_n and $k_{d,n}$ are the fractile factors for the characteristic and ULS design values, respectively, taking into account the available number of samples n from experimental tests, also known in the scientific literature as tolerance factors [23]. The numerical values of k_n and $k_{d,n}$ coefficients

Table 2
Mean, standard deviation and coefficient of variation from experiments, best-fit Gaussian, Weibull and Lognormal distributions of the key design variables.

		Experimental			Gaussian			Weibull			Lognormal		
		m_{exp}	s_{exp}	COV_{exp}	m_G	s_G	COV_G	m_W	s_W	COV_W	m_L	s_L	COV_L
Effective area [mm²]	0°	27.03	2.98	11 %	27.03	3.14	12 %	26.98	3.30	12 %	27.05	3.17	12 %
	10°	26.55	1.67	6 %	26.55	1.76	7 %	26.42	2.17	8 %	26.55	1.74	7 %
	45°	32.87	2.48	8 %	32.86	2.6	8 %	32.85	2.64	8 %	32.88	2.63	8 %
Yield strength [kN]	0°	7.07	0.50	7 %	7.07	0.53	7 %	7.04	0.61	9 %	7.07	0.52	7 %
	10°	6.85	0.40	6 %	6.79	0.38	6 %	6.84	0.42	6 %	6.79	0.38	6 %
	45°	6.33	0.50	8 %	6.33	0.50	8 %	6.35	0.35	6 %	6.33	0.54	8 %
Ultimate strength [kN]	0°	14.91	0.93	6 %	14.91	0.93	6 %	14.98	0.52	3 %	14.91	0.93	6 %
	10°	14.75	0.41	3 %	14.75	0.41	3 %	14.98	0.52	3 %	14.75	0.41	3 %
	45°	13.15	0.98	7 %	13.15	0.98	7 %	13.18	0.81	6 %	13.15	0.98	7 %

are reported in Table D1 and Table D2 of [19] for the characteristic and ULS design values, respectively. Two different cases are provided, related to the prior knowledge of the variable: "*COV known*" (*K*) is applicable if prior tests are available or if the COV can be reasonably predicted using engineering judgment; "*COV unknown*" (*UK*) applies when no prior knowledge is available and the COV cannot be predicted. Hereafter, the two EC0 approaches are distinguished using the following acronyms, namely EC0-K and EC0-UK. The evaluation of m_y and s_y are: $m_y = \frac{1}{n}\sum_{i=1}^{n}\ln(x_i)$, $s_y = \sqrt{\frac{1}{n-1}\sum_{i=1}^{n}\left(\ln(x_i) - m_y\right)^2}$ for EC0-UK, while $s_y = V_x$ for EC0-K, where x_i represents the strength of the *i*-th specimen and V_x is the COV of the sample.

It is worth noticing that the tolerance factor values suggested by EC0 were derived using a Bayesian approach with "vague" prior distributions, that should lead to almost the same results as classical statistics with confidence levels equal to 75 %.

The characteristic and ULS design values of the yield and ultimate tensile strengths estimated according to the EC0 approach will be referred to as $f_{y,k-EC0}, f_{y,d-EC0}, f_{u,k-EC0}, f_{u,d-EC0}$. The corresponding partial safety factors can be computed as follows:

$$\gamma_{M-EC0} = \frac{x_{k-EC0}}{x_{d-EC0}} \tag{12}$$

The strength hardening ratios, defined as the ratio between ultimate tensile strength and yield strength, can be computed for the characteristic and ULS design values as follows:

$$\eta_{k-EC0} = \frac{f_{u,k}}{f_{y,k}} \tag{13}$$

$$\eta_{d-EC0} = \frac{f_{u,d}}{f_{y,d}} \tag{14}$$

Finally, the material overstrength factor is defined as the ratio between the mean and the characteristic value of the strength as follows:

$$\gamma_{0v-EC0} = \frac{m_L}{x_{k-EC0}} \tag{15}$$

Table 3
Kolmogorov-Smirnov test of the Gaussian, Lognormal and Weibull best fit statistical distributions.

		Kolmogorov-Smirnov test			Akaike information criterion		
		KS_G [-]	KS_W [-]	KS_L [-]	AIC_G [-]	AIC_W [-]	AIC_L [-]
Effective area	0°	0.230	0.270	0.220	54.22	54.92	54.17
	10°	0.210	0.252	0.198	42.61	44.97	42.32
	45°	0.170	0.170	0.173	45.85	45.98	45.96
Yield resistance	0°	0.210	0.201	0.223	18.47	20.09	18.29
	10°	0.181	0.170	0.184	12.84	13.17	12.88
	45°	0.270	0.157	0.291	15.96	11.61	17.26
Ultimate resistance	0°	0.326	0.305	0.333	29.90	21.82	31.38
	10°	0.159	0.135	0.158	13.65	12.59	13.80
	45°	0.225	0.164	0.235	28.04	25.88	28.67

4.2. CL approach

The CL based approach here proposed allows to estimate the percentile of a given CL based on the knowledge of the best-fit distribution derived from a sample of size *n*. Two different formulations are here implemented [30,43]. The first one is applicable when the experimental distribution follows a Gaussian distribution, while the second one is applicable for a generic best-fit distribution. As mentioned, the 5 %-percentile CL is used to estimate the characteristic design value, while the 0.1 %-percentile CL is employed to estimate the ULS design value.

In detail, the first formulation based on the best-fit Gaussian distribution and hereafter referred to as "CL-G" allows to estimate the two-sided 100•(1-α)% confidence interval, hereafter simply referred to as CI, of $x_{p\text{-}G}$, namely $\left[\underline{x_{p-G}}, \overline{x_{p-G}}\right]$. The suffix *p-G* indicates the *p*-percentile of the best-fit Gaussian distribution, while $\widehat{x_{p-G}}$ represents the central value of the CI. The CI can be estimated according to the following formulation:

$$\left[\underline{x_{p-G}}, \overline{x_{p-G}}\right] = \left[m_{\exp} - t_{(1-\alpha/2;n-1,\delta)}\frac{s_{\exp}}{\sqrt{n}}, m_{\exp} - t_{(\alpha/2;n-1,\delta)}\frac{s_{\exp}}{\sqrt{n}}\right] \tag{16}$$

The term $t_{(\gamma;n-1,\delta)}$ is the γ-percentile of a noncentral t-distribution with *n*-1 degrees of freedom and non-centrality parameter $\delta = -\sqrt{n}z_{(p)} = \sqrt{n}z_{(1-p)}$, where *z(p)* is the CDF value of the standard normal Gaussian distribution corresponding to a probability equal to *p*.

The second formulation based on the best-fit Lognormal distributions hereafter referred to as "CL-LN" allows the estimation of the two-sided 100•(1-α)% CI for $x_{p\text{-}LN}$, namely $\left[\underline{x_{p-LN}}, \overline{x_{p-LN}}\right]$. The suffix *p-LN* indicates the *p*-percentile of the best-fit Lognormal distribution, while $\widehat{x_{p-LN}}$ represents the central value of the CI. The CI can be estimated according to the following formulation:

$$\left[\underline{x_{p-LN}}, \overline{x_{p-LN}}\right] = \left[\widehat{x_{p-LN}} - k \bullet se\left(\widehat{x_p}\right), \widehat{x_p} + k \bullet se\left(\widehat{x_p}\right)\right] \tag{17}$$

Where $se\widehat{x_p}$ is the estimation of the standard error of $\widehat{x_{p-LN}}$ and can be evaluated according to the following expression:

$$se\left(\widehat{x_{p-LN}}\right) = \sqrt{\frac{p(1-p)}{n \bullet f_{LN}\left(\widehat{x_p}\right)^2}} \tag{18}$$

The characteristic and ULS design values of yield and ultimate tensile strengths estimated according to the CL approach, and hereafter referred to as $f_{y,k-CL}$, $f_{y,d-CL}$, $f_{u,k-CL}$, $f_{u,d-CL}$ respectively, are taken as the lower bounds of each considered CI. The material partial safety factors for the considered state (either yielding or ultimate condition) can be estimated as follows:

$$\gamma_{M-CL} = \frac{x_{k-CL}}{x_{d-CL}} \tag{19}$$

The strength hardening ratios, defined as the ratio between ultimate

tensile strength and yield strength, can be computed considering both the characteristic and ULS strengths:

$$\eta_{k-CL} = \frac{f_{u,k-CL}}{f_{y,k-CL}} \tag{20}$$

$$\eta_{d-CL} = \frac{f_{u,d-CL}}{f_{y,d-CL}} \tag{21}$$

Finally, the material overstrength factors are defined as the ratio between the mean and the characteristic value as follows:

$$\gamma_{0v-CL} = \frac{m}{x_{k-CL}} \tag{22}$$

5. Main results from the calibration analysis

This section presents the results of the calibration analysis conducted according to the EC0 and CL approaches introduced in the previous section. Both cases of known (K) and unknown (UK) COV are encompassed when considering the EC0 approach, while five different CI amplitudes are considered for the CL approach, corresponding to 1-α values equal to 95 %, 90 %, 84 %, 75 % and 50 %, respectively. Additionally, the central value of the CI ($\widehat{x_p}$) are also computed. These values correspond to either the 5 % percentile (when considering the characteristic value) or the 0.1 % percentile (when considering the ULS design value).

As mentioned before, four distinct samples are considered, the first three ones coinciding with the individual batches (dot-0, dot-10 and dot-45), while the fourth one corresponding to the merging of dot-0 and dot-10 batches. The rationale behind the merging of dot-0 and dot-10 batches is the similar tensile behavior, as discussed in Section 2. The aim of the statistical analysis performed on the merged sample is to assess the influence of the sample size (the first three samples having a size of 10, 10 and 9 specimens, respectively, while the fourth sample having a size of 20 specimens) on the design values, material partial safety factors, material overstrength factors and strength hardening ratios. In detail, Section 5.1 presents the main results from the calibration study, while further discussions oriented to design purposes are provided in Section 5.2.

5.1. Design values and partial safety factors

The main results of the calibration analysis are summarized in the tables and graphs included, for sake of conciseness, in Annexes 2 and 3. First, Tables A1 and A2 in Annex 2 provide the numerical values of the yield and ultimate strengths, and corresponding safety factors according to the EC0 approach, while Tables A3 and A4 in Annex 2 provide the main results on yield and ultimate strengths and corresponding safety factors according to the CL approach. Then, the trends of the design strength values (both characteristic and ULS values) and related partial safety factors, strength hardening ratios and material overstrength factors are graphically represented through the bar charts and graphs shown in Figures A3-A9 in Annex 3. The following trends and general observations result from the analysis of these tables and graphs:

- As expected, the design values estimated according to the CL approach decrease as the CI amplitude 1-α increases. For the four considered samples, the CL design values are always smaller than the corresponding EC0 design values. Moreover, in most cases, the EC0 characteristic and ULS design values are higher than the corresponding percentiles (e.g. 5 % percentile and 0.1 % percentile, respectively). Clearly, this is a trivial result when considering the CL-LN design values since they are based on the Lognormal distribution, as for the EC0 design values. However this is not obvious for the CL-G design values. In general, the CL-LN design values at 50 % CI are very close to the corresponding EC0-UK values.
- Both the 0.1 % and 5 % percentiles of the Gaussian distributions (e.g., $\widehat{x_{0.1\%-G}}$ and $\widehat{x_{5\%-G}}$) are smaller than the corresponding ones as obtained considering the LN distributions (e.g., $\widehat{x_{0.1\%-LN}}$ and $\widehat{x_{5\%-LN}}$).
- The CL-LN ULS design values are smaller than the corresponding CL-G values. However, an opposite trend is observed instead for the characteristic values, since CL-G characteristic values are smaller than the corresponding CL-LN values.
- The partial factors for yield and ultimate strengths are between 1.14-1.93 and 1.06-1.83, respectively. As expected, the larger values are obtained for the dot-45 sample, being characterized by higher COV.
- The partial factors obtained considering the CL-G and CL-LN approaches are higher than the corresponding ones considering both EC0-K and EC0-UK approaches. In particular, the values of the partial safety factors according to the CL-G approach considering 1-α = 50 % are quite close to the ones corresponding EC0-UK values.

The trends of the strength hardening ratios η_k and η_d for the characteristic and ULS design values computed according to the EC0 and CL approaches are shown in the graphs of Figure A8 in Annex 3. Overall, the numerical values are less affected by the increasing build direction and tend to be higher for the ULS design values. In detail, the numerical values of η_k are between 2.10 and 2.43 for the CL approach, in line with the EC0 values, with the highest values and variability observed for the dot-10 batch. The numerical values of η_d show higher variability ranging between 2.13 and 2.99 for the CL appraoch, and between 2.11 and 2.47 for the EC0 approach, with the highest values observed, again, for the dot-10 sample. These values are significantly higher than the values of around 1.2 and 1.4 exhibited by WAAM carbon steel but are consistent with the values of 2.2 to 2.4 for stainless steel, computed based on the minimum specified strength [44]. This result depends on the hardening effect evidenced by the tensile tests on WAAM stainless steel bars (see e.g. [29]).

The trends of the overstrength factors γ_{0v} for the yield and ultimate strengths computed according to the EC0 and CL approaches are shown in the graphs of Figure A9 in Annex 3. Overall, the numerical values are between 1.12 and 1.40 for yield strengths and are moderately affected by the build direction. The same trend is exhibited by the values of overstrength factor for the ultimate strengths which range from 1.06 and 1.37. The higher values are evidenced by the $\gamma_{0v,y}$ and $\gamma_{0v,u}$ of the dot-45 sample, being the one with the largest variability. These values are close to the overstrength factor of 1.3 specified for structural steel in EC3 and aligned with the values for stainless steel, where mean strength factors of 1.25 for yield strength and 1.14 for ultimate strength were observed, as presented in [45].

5.2. Discussion on design values with respect to Eurocode provisions

This section discusses the main results obtained from the calibration study presented in Section 5.1 in light of potential implications from structural design perspectives.

Firstly, it is very important to highlight that the results presented here are based on a limited number of samples and therefore are characterized by large uncertainty. Secondly, these values can be considered representative and valid only for the investigated WAAM process and for the current state of development of the dot-by-dot deposition strategy. Therefore, additional data and experimental tests need to be performed in order to increase the reliability, the range of validity and robustness of the obtained numerical results. Indeed, other manufacturers should be considered and the influence of printing parameters in the mechanical response should be evaluated in depth.

Overall, despite the necessary remarks related to the limited validity of the present results, the work provides first data regarding design values and material partial safety factors for dot-by-dot WAAM stainless steel. The main findings in terms of design values for yield and ultimate

Table 4
Comparison between design values for dot-by-dot WAAM stainless steel bars (CL approach for 75 % CI and EC0-UK approach) and conventional stainless steel and carbon steel S235 from EC3.

Mechanical parameter	Batch	CL-LN 75 % (from the present work)	EC0-UK (from the present work)	EC3 stainless steel *	EC3 carbon steel S235
f_{yk} [MPa]	dot−0	210	216	210	235
	dot−10	210	216		
	dot−45	184	189		
f_{yd} [MPa]	dot−0	153	179	191	224
	dot−10	162	186		
	dot−45	126	149		
γ_{M0} [-]	dot−0	1.38	1.21	1.10	1.05
	dot−10	1.30	1.16		
	dot−45	1.46	1.27		
f_{uk} [MPa]	dot−0	453	463	520	360
	dot−10	487	494		
	dot−45	387	399		
f_{ud} [MPa]	dot−0	343	388	416	288
	dot−10	433	459		
	dot−45	272	321		
γ_{M2} [-]	dot−0	1.32	1.19	1.25	1.25
	dot−10	1.13	1.08		
	dot−45	1.42	1.24		
$\gamma_{0v,y}$ [-]	dot−0	1.19	1.16	n.a.	1.30 * *
	dot−10	1.14	1.11		
	dot−45	1.21	1.18		
$\gamma_{0v,u}$ [-]	dot−0	1.16	1.14	n.a.	
	dot−10	1.07	1.06		
	dot−45	1.20	1.17		

*The equivalent grade is assumed as austenitic steel grade 1.4301.
* *EC8 states that reference should be made to the National Annex for the applicable values

tensile strengths and strength-related parameters are summarized in Table 4 and compared with the current design values of conventionally produced 304 L stainless steel material and S235 carbon steel as provided by EC3 for structural applications. In detail, Table 4 compares the results of the present work provided by both the EC0-UK approach and the CL-LN approach with CI= 75 %.

Overall, it can be noticed that both the characteristic and ULS design values for the yield strength of dot-by-dot WAAM bars obtained from the present work are slightly less than the ones provided by EC3 for both stainless and carbon steels. On the contrary, the characteristic and ULS design values for the ultimate tensile strength of dot-by-dot WAAM bars obtained from the present work are in general higher the those provided by EC3 for S235 carbon steel, but lower than those provided by EC3 for 304L stainless steel.

The values of γ_{M0} material partial safety factor obtained from the present work are, in general, higher than those provided by EC3 for stainless steel and S235 carbon steel, while the values of γ_{M2} material safety factors exhert high variability around values provided by EC3. The values of γ_{0v} overstrength factors are slightly lower than those provided by EC3.

6. Conclusions

The present work provides insights into the tensile behaviour of dot-by-dot WAAM-produced stainless steel bars with the aim of calibrating the design values of yield and ultimate tensile strength and corresponding material partial safety factors, overstrength and strength hardening ratios, accounting for the influence of the build angle and the limited sample size. From the results presented in this work, some final considerations can be drawn:

- The coupling of the main inherent geometrical irregularities and stainless steel material properties leads to a marked anisotropy with an evident hardening response, exhibiting also large variability (e.g. COV) within the same batch of production. Such behavior is reflected in the experimental distributions of the main geometrical and resistance variables considered, which are characterized by COV values in the range of 5-10 % when considering the effective cross-sectional area, and up to 20 % when considering the resistance parameters.
- The correlation analysis between the resistance variables and the effective cross-sectional area (corresponding to a volume-equivalent integral measure of the area of the printed bar) revealed that both the yield and ultimate tensile resistances are very weakly correlated with the effective area. This result indicates that the level of reliability of an assessment of resistance values based on nominal stress (i.e. stress calculated considering nominal cross-sectional areas) would be similar to the one based on the use of effective cross-sectional areas, whose evaluation requires, however, an additional effort and specific measurements. Thus the use of nominal stress values is suggested for design purposes.
- The comparison between the two calibration approaches for the strength design values and related material partial safety factors, overstrength factors and strength hardening ratios reveal that the approach based on the confidence level (CL) may result in quite smaller values than those estimated according to the "design assisted by testing" approach of EC0. Overall, the design values are either slightly smaller or comparable to the values of conventional 304 L stainless and S235 carbon steels, as provided by current EC3 provisions. However, for the specific dot-by-dot WAAM technology investigated in this work, the strength design values significantly reduce with increasing build angle (i.e. 45°). As a consequence, the calibrated values of the material partial safety factors, especially for γ_{M0} material partial safety factor, tend to be higher than those provided by EC3 for conventional structural stainless and carbon steels.

Finally, it is important to highlight that the quantitative results presented here are based on samples of quite limited size, and are therefore characterized by an intrinsicly high uncertainty. Hence, their validity is maintained only for the investigated dot-by-dot WAAM process (i.e. set of specific process parameters) and for the current state of development of the dot-by-dot WAAM technology.

CRediT authorship contribution statement

Tomaso Trombetti: Supervision. **Michele Palermo:** Conceptualization, Investigation, Visualization, Writing – original draft. **Giada Gasparini:** Resources, Writing – review & editing. **Lidiana Arrè:** Investigation, Visualization. **Vittoria Laghi:** Conceptualization, Investigation, Writing – original draft.

Declaration of Competing Interest

The authors declare that they have no known competing financial interests or personal relationships that could have appeared to influence the work reported in this paper.

Acknowledgements

The support of Dutch company MX3D held in Amsterdam is gratefully acknowledged for giving the additive-manufactured elements tested.

Dr. Vittoria Laghi gratefully acknowledges the financial support of "Young Researchers" – Seal of Excellence 2022 grant - funded on D.M. 737/2021 resources-funded by European Union –"NextGenerationEU".

The authors gratefully acknowledge the financial support provided through the LATTICE Project (Research Project of National Interest, PRIN 2022P7FLNC) funded by the Italian Ministry of University and Research (MUR).

Appendix

Annex 1: Graphs from statistical analysis

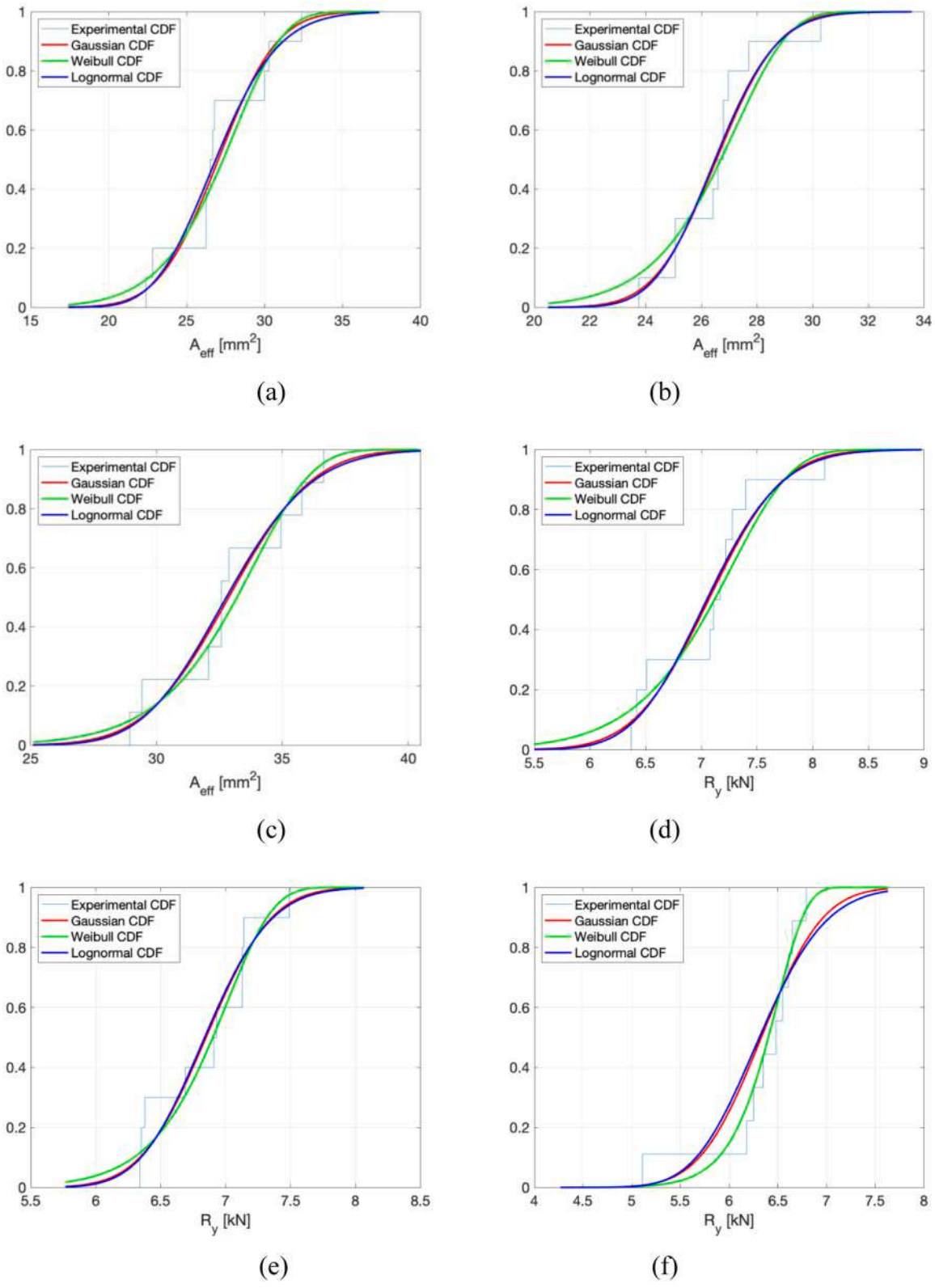

Fig. A1. CDF of effective cross-sectional area: (a) for dot-0, (b) dot-10 and (c) dot-45 specimens. CDF of yield resistance: (d) for dot-0, (e) dot-10 and (f) dot-45 specimens. CDF of ultimate resistance: (g) for dot-0, (h) dot-10 and (i) dot-45 specimens.

.

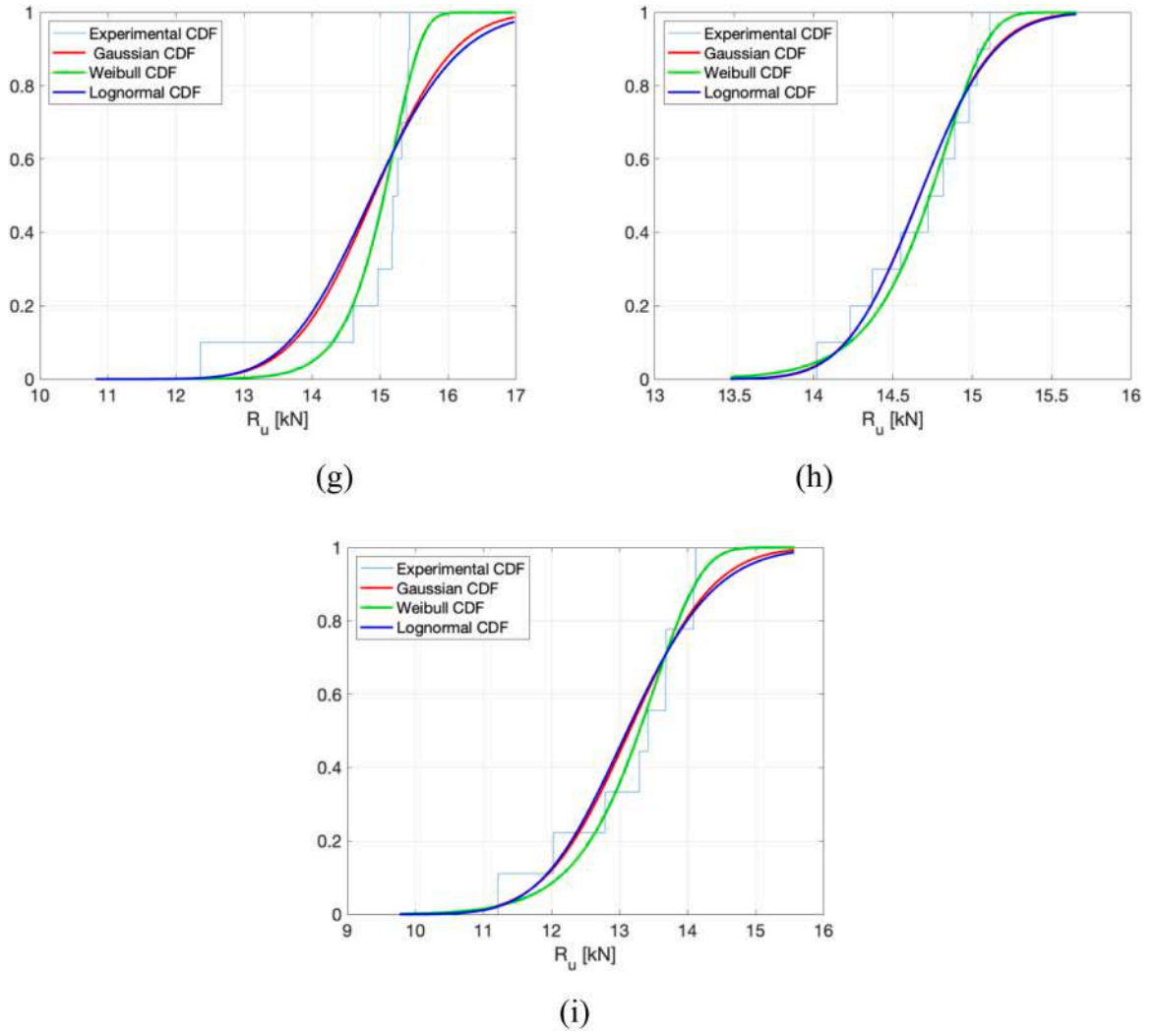

Fig. A1. (*continued*).

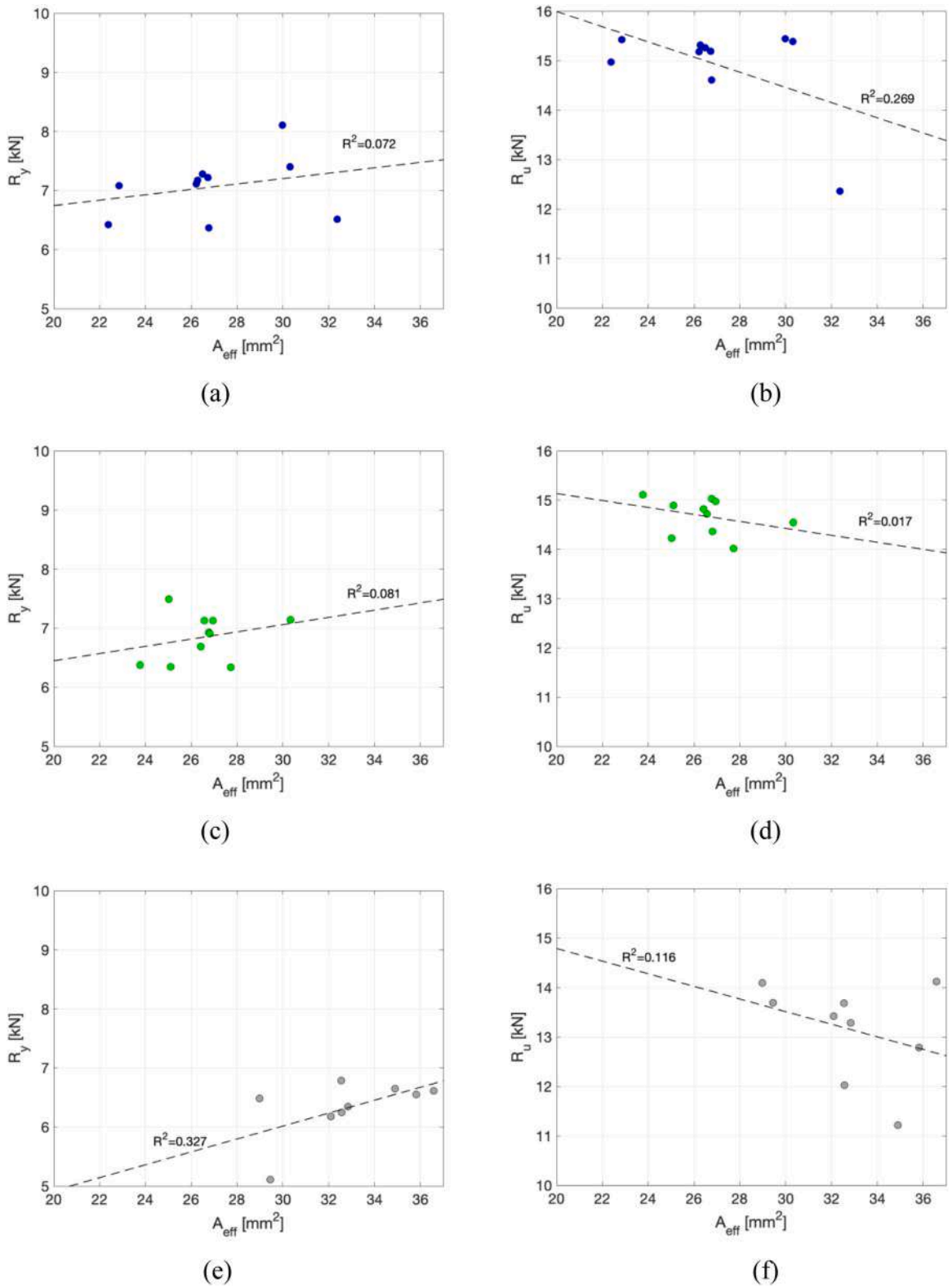

Fig. A2. Correlation plots between yield resistance and effective cross-sectional area for (a) dot-0, (c) dot-10 and (e) dot-45 specimens. Correlation plots between ultimate resistance and effective cross-sectional area for (b) dot-0, (d) dot-10 and (f) dot-45 specimens.

.

Annex 2: Tables from the calibration analysis

Table A1
Characteristic and ULS design values for the yield strengths and corresponding safety factors according to EC0 approach.

		Design values		
Batch	**Prior knowledge**	**$f_{y,k}$ [MPa]**	**$f_{y,d}$ [MPa]**	γ_{M0}
Dot−0	UK	216	179	1.21
	K	220	196	1.12
Dot−10	UK	216	186	1.16
	K	219	200	1.09
Dot−45	UK	189	149	1.27
	K	195	173	1.13
Dot−0 +Dot−10	UK	218	193	1.13
	K	219	199	1.10

Table A2
Characteristic and ULS design values for the ultimate strengths and corresponding safety factors according to EC0 approach.

		Design values		
Batch	**Prior knowledge**	**$f_{u,k}$ [MPa]**	**$f_{u,d}$ [MPa]**	γ_{M2}
Dot−0	UK	463	388	1.19
	K	473	430	1.10
Dot−10	UK	494	459	1.08
	K	497	476	1.04
Dot−45	UK	399	321	1.24
	K	408	364	1.12
Dot−0 +Dot−10	UK	479	436	1.10
	K	484	451	1.07

Table A3
Characteristic and ULS design values for the yield strengths and corresponding partial factors according to CL approach and the percentiles.

Batch	Characteristic and Design values		Confidence Interval						
				95%	90%	84%	75%	50%	Percentile
Dot−0	Strength	$f_{y,k}$ G [MPa]	L	189	196	200	204	211	221
			U	233	231	230	228	224	
		$f_{y,k}$ LN [MPa]	L	202	205	208	210	215	223
			U	243	240	237	234	230	
		$f_{y,d}$ G [MPa]	L	142	153	160	167	178	195
			U	213	210	208	205	200	
		$f_{y,d}$ LN [MPa]	L	118	132	142	153	173	201
			U	283	270	260	249	229	
	Partial factor	$\gamma_{M0\text{-}G}$		1.33	1.28	1.25	1.22	1.18	1.13
		$\gamma_{M0\text{-}LN}$		1.70	1.56	1.47	1.38	1.25	1.11
Dot−10	Strength	$f_{y,k}$ G [MPa]	L	194	199	202	205	211	219
			U	228	227	226	225	222	
		$f_{y,k}$ LN [MPa]	L	203	206	208	210	214	220
			U	237	234	232	230	226	
		$f_{y,d}$ G [MPa]	L	156	165	170	176	185	199
			U	212	210	208	206	202	
		$f_{y,d}$ LN [MPa]	L	134	145	153	162	179	202
			U	271	260	251	242	226	
	Partial factor	$\gamma_{M0\text{-}G}$		1.24	1.21	1.19	1.17	1.14	1.10
		$\gamma_{M0\text{-}LN}$		1.52	1.42	1.36	1.30	1.20	1.09
Dot−45	Strength	$f_{y,k}$ G [MPa]	L	160	167	172	176	184	195
			U	207	205	204	202	198	
		$f_{y,k}$ LN [MPa]	L	175	179	181	184	189	197
			U	218	214	212	209	204	
		$f_{y,d}$ G [MPa]	L	110	122	131	138	150	169
			U	187	184	182	179	174	
		$f_{y,d}$ LN [MPa]	L	91	104	115	126	146	175
			U	260	247	236	225	204	
	Partial factor	$\gamma_{M0\text{-}G}$		1.45	1.36	1.32	1.28	1.22	1.15
		$\gamma_{M0\text{-}LN}$		1.93	1.71	1.58	1.46	1.29	1.13
Dot−0 +Dot−10	Strength	$f_{y,k}$ G [MPa]	L	202	205	208	210	213	219
			U	227	226	225	224	221	
		$f_{y,k}$ LN [MPa]	L	207	209	210	212	216	220
			U	234	232	230	228	225	

(*continued on next page*)

Table A3 (*continued*)

Batch	Characteristic and Design values		Confidence Interval						
				95%	90%	84%	75%	50%	Percentile
		$f_{y,d}$ G [MPa]	L	168	173	176	180	186	195
			U	208	206	204	202	199	
		$f_{y,d}$ LN [MPa]	L	145	154	160	168	181	200
			U	255	246	239	232	219	
	Partial factor	$\gamma_{M0\text{-}G}$		1.21	1.19	1.18	1.17	1.15	1.12
		$\gamma_{M0\text{-}LN}$		1.42	1.36	1.31	1.27	1.19	1.1

Table A4
Characteristic and ULS design values for the ultimate strengths and corresponding partial factors according to CL approach and the percentiles.

Batch	Characteristic and Design values		Confidence Interval						
				95%	90%	84%	75%	50%	Percentile
Dot−0	Strength	$f_{u,k}$ G [MPa]	L	415	427	434	442	454	473
			U	496	492	489	486	480	
		$f_{u,k}$ LN [MPa]	L	437	444	448	453	463	476
			U	515	508	504	499	489	
		$f_{u,d}$ G [MPa]	L	326	347	360	373	394	426
			U	458	453	449	444	434	
		$f_{u,d}$ LN [MPa]	L	278	303	322	343	381	435
			U	592	567	548	527	489	
	Partial factor	$\gamma_{M2\text{-}G}$		1.27	1.23	1.21	1.18	1.15	1.11
		$\gamma_{M2\text{-}LN}$		1.57	1.46	1.39	1.32	1.21	1.09
Dot−10	Strength	$f_{u,k}$ G [MPa]	L	471	477	480	484	489	498
			U	508	506	505	503	500	
		$f_{u,k}$ LN [MPa]	L	480	483	485	487	492	498
			U	516	514	511	509	504	
		$f_{u,d}$ G [MPa]	L	432	441	447	453	462	476
			U	491	488	487	485	480	
		$f_{u,d}$ LN [MPa]	L	400	413	422	433	451	478
			U	556	544	534	524	505	
	Partial factor	$\gamma_{M2\text{-}G}$		1.09	1.08	1.07	1.07	1.06	1.05
		$\gamma_{M2\text{-}LN}$		1.20	1.17	1.15	1.13	1.09	1.04
Dot−45	Strength	$f_{u,k}$ G [MPa]	L	340	354	363	372	387	408
			U	433	429	426	422	415	
		$f_{u,k}$ LN [MPa]	L	370	376	381	387	397	412
			U	453	447	442	436	426	
		$f_{u,d}$ G [MPa]	L	242	267	283	298	321	358
			U	393	388	383	378	367	
		$f_{u,d}$ LN [MPa]	L	202	229	249	272	312	370
			U	537	510	490	468	427	
	Partial factor	$\gamma_{M2\text{-}G}$		1.40	1.33	1.29	1.25	1.20	1.14
		$\gamma_{M2\text{-}LN}$		1.83	1.64	1.53	1.42	1.27	1.11
Dot−0 +Dot−10	Strength	$f_{u,k}$ G [MPa]	L	458	463	466	470	475	483
			U	497	494	493	491	487	
		$f_{u,k}$ LN [MPa]	L	464	467	470	473	478	485
			U	506	503	500	498	492	
		$f_{u,d}$ G [MPa]	L	406	414	419	424	433	447
			U	467	464	461	458	453	
		$f_{u,d}$ LN [MPa]	L	364	379	389	401	422	453
			U	541	527	516	505	483	
	Partial factor	$\gamma_{M2\text{-}G}$		1.13	1.12	1.11	1.11	1.10	1.08
		$\gamma_{M2\text{-}LN}$		1.27	1.23	1.21	1.18	1.13	1.07

Table A5
Characteristic and ULS design values for the strength hardening ratios (η_k and η_d) according to CL approach and the percentiles.

Batch	Strength hardening ratio [-]	Confidence Interval					
		95%	90%	84%	75%	50%	Percentile
Dot−0	$\eta_{k\text{-}CL}$ G	2.19	2.18	2.17	2.17	2.16	2.14
	$\eta_{k\text{-}CL}$ LN	2.16	2.16	2.15	2.15	2.15	2.13
	$\eta_{d\text{-}CL}$ G	2.30	2.27	2.25	2.23	2.21	2.18
	$\eta_{d\text{-}CL}$ LN	2.35	2.30	2.27	2.24	2.21	2.16
Dot−10	$\eta_{k\text{-}CL}$ G	2.43	2.40	2.37	2.35	2.32	2.27
	$\eta_{k\text{-}CL}$ LN	2.36	2.35	2.33	2.32	2.30	2.26
	$\eta_{d\text{-}CL}$ G	2.77	2.68	2.62	2.57	2.50	2.39
	$\eta_{d\text{-}CL}$ LN	2.99	2.85	2.76	2.67	2.53	2.37
Dot−45	$\eta_{k\text{-}CL}$ G	2.13	2.12	2.11	2.11	2.11	2.09
	$\eta_{k\text{-}CL}$ LN	2.11	2.11	2.10	2.10	2.10	2.09
	$\eta_{d\text{-}CL}$ G	2.20	2.18	2.17	2.15	2.14	2.12
	$\eta_{d\text{-}CL}$ LN	2.23	2.20	2.18	2.16	2.13	2.11
Dot−0 +Dot−10	$\eta_{k\text{-}CL}$ G	2.27	2.25	2.25	2.24	2.23	2.21
	$\eta_{k\text{-}CL}$ LN	2.24	2.24	2.23	2.23	2.21	2.20
	$\eta_{d\text{-}CL}$ G	2.42	2.40	2.38	2.36	2.33	2.29
	$\eta_{d\text{-}CL}$ LN	2.51	2.46	2.43	2.39	2.33	2.27

Table A6
Characteristic and ULS design values for the material overstrength factors (γ_{0V}) according to CL approach and the percentiles.

Batch	Material overstrength factor [-]	Confidence Interval					
		95%	90%	84%	75%	50%	Percentile
Dot−0	$\gamma_{0v,y\text{-}CL}$ G	1.32	1.28	1.25	1.22	1.19	1.13
	$\gamma_{0v,y\text{-}CL}$ LN	1.24	1.22	1.20	1.19	1.16	1.12
	$\gamma_{0v,u\text{-}CL}$ G	1.27	1.24	1.21	1.19	1.16	1.11
	$\gamma_{0v,u\text{-}CL}$ LN	1.21	1.19	1.18	1.16	1.14	1.11
Dot−10	$\gamma_{0v,y\text{-}CL}$ G	1.24	1.21	1.19	1.17	1.14	1.10
	$\gamma_{0v,y\text{-}CL}$ LN	1.18	1.17	1.15	1.14	1.12	1.09
	$\gamma_{0v,u\text{-}CL}$ G	1.11	1.09	1.09	1.08	1.07	1.05
	$\gamma_{0v,u\text{-}CL}$ LN	1.09	1.08	1.08	1.07	1.06	1.05
Dot−45	$\gamma_{0v,y\text{-}CL}$ G	1.40	1.34	1.30	1.27	1.22	1.15
	$\gamma_{0v,y\text{-}CL}$ LN	1.28	1.25	1.23	1.21	1.18	1.14
	$\gamma_{0v,u\text{-}CL}$ G	1.37	1.31	1.28	1.25	1.20	1.14
	$\gamma_{0v,u\text{-}CL}$ LN	1.26	1.24	1.22	1.20	1.17	1.13
Dot−0 +Dot−10	$\gamma_{0v,y\text{-}CL}$ G	1.22	1.20	1.19	1.17	1.15	1.12
	$\gamma_{0v,y\text{-}CL}$ LN	1.19	1.18	1.17	1.16	1.14	1.12
	$\gamma_{0v,u\text{-}CL}$ G	1.14	1.13	1.13	1.12	1.10	1.09
	$\gamma_{0v,u\text{-}CL}$ LN	1.13	1.12	1.12	1.11	1.10	1.08

Annex 3: Graphs from the calibration analysis

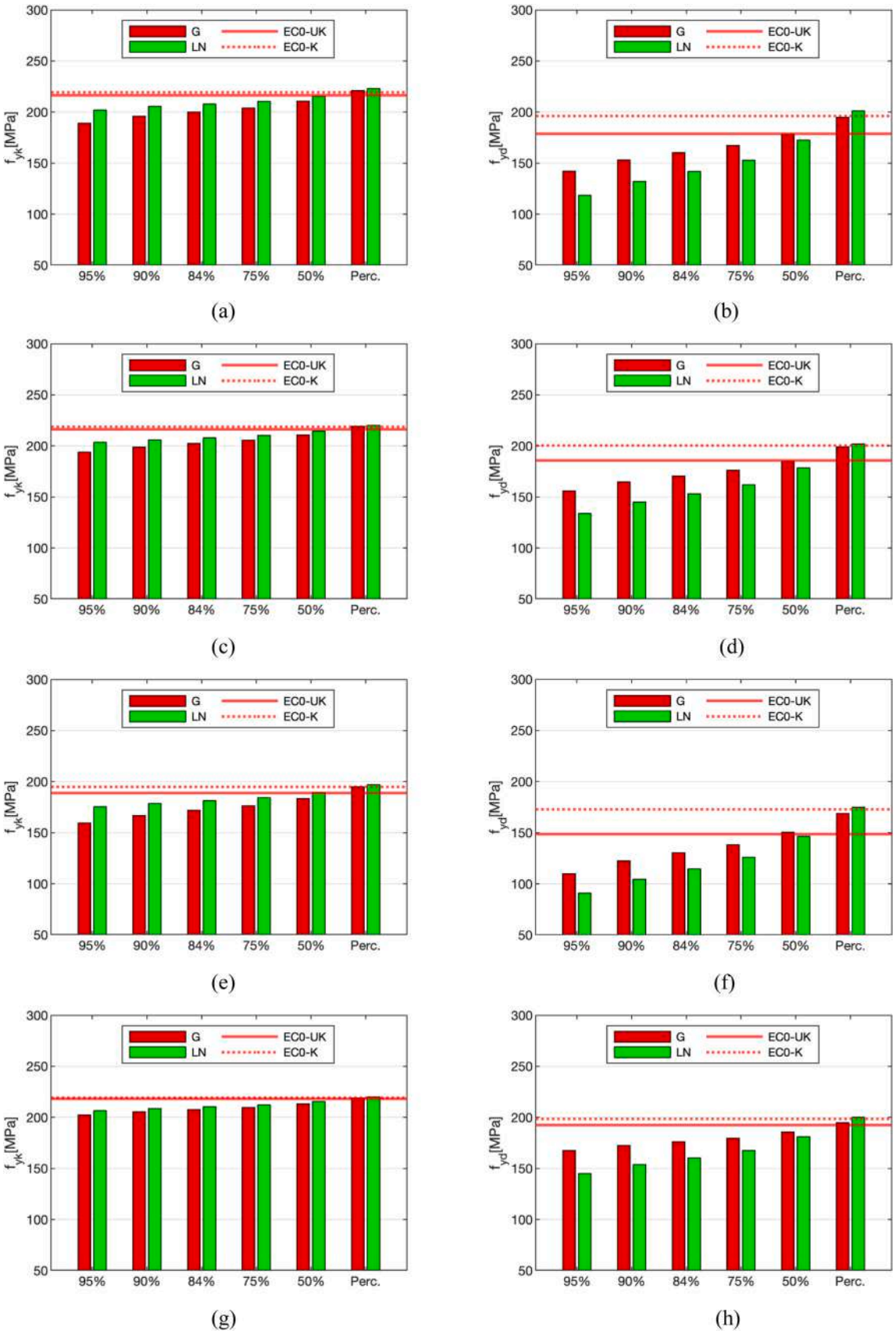

Fig. A3. Bar charts representing the yield strength according to CL approach (for the different CI amplitudes), EC0 approach and the percentiles: (a) dot-0 (f_{yk}), (b) dot-0 (f_{yd}), (c) dot-10 (f_{yk}), (d) dot-10 (f_{yd}), (e) dot-45 (f_{yk}), (f) dot-45 (f_{yd}), (g) dot-0&10 (f_{yk}), (h) dot-0&10 (f_{yd}).

.

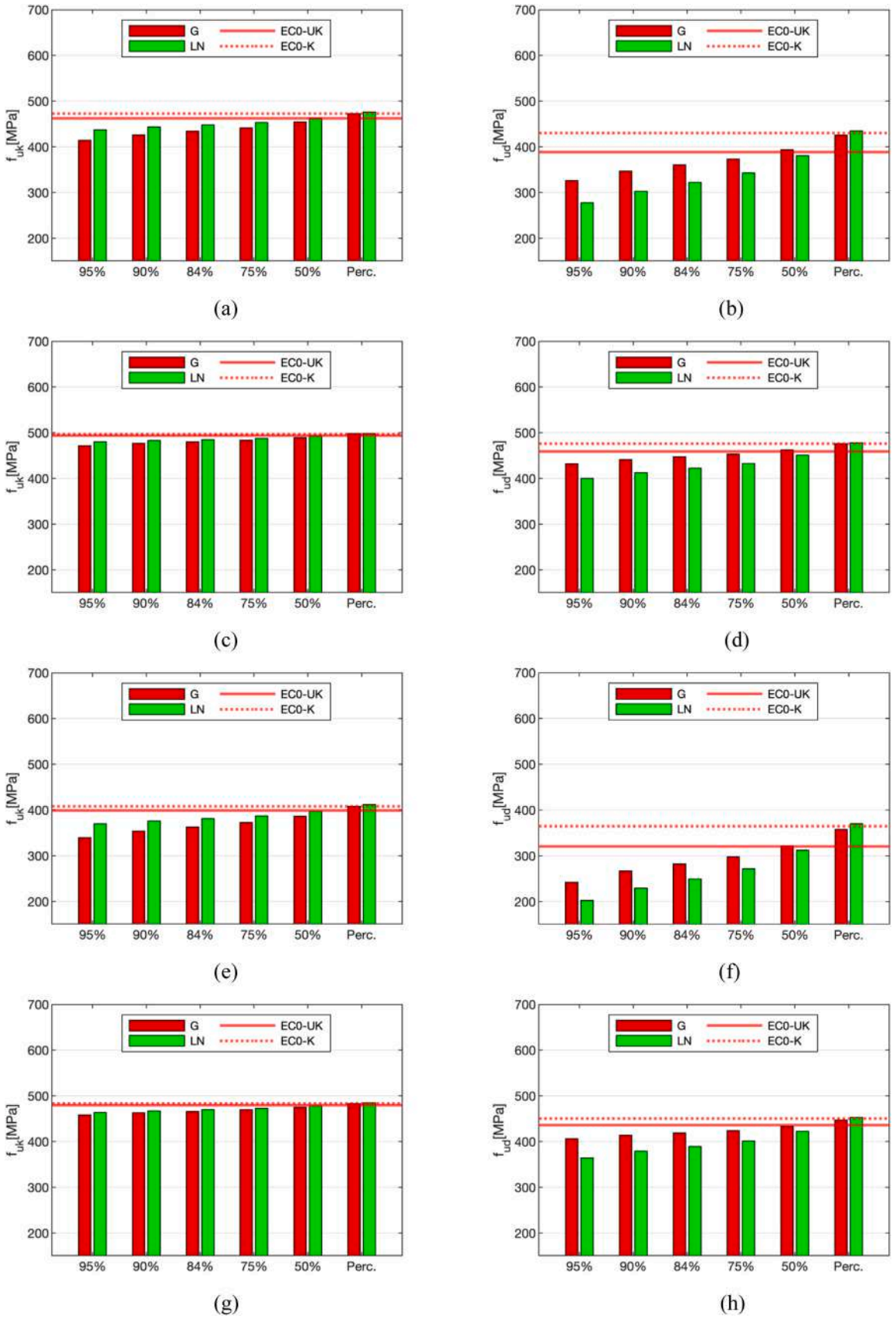

Fig. A4. Bar charts representing the ultimate strength according to CL approach (for the different CI amplitudes), EC0 approach and the percentiles: (a) dot-0 (f_{yk}), (b) dot-0 (f_{yd}), (c) dot-10 (f_{yk}), (d) dot-10 (f_{yd}), (e) dot-45 (f_{yk}), (f) dot-45 (f_{yd}), (g) dot-0&10 (f_{yk}), (h) dot-0&10 (f_{yd}).

.

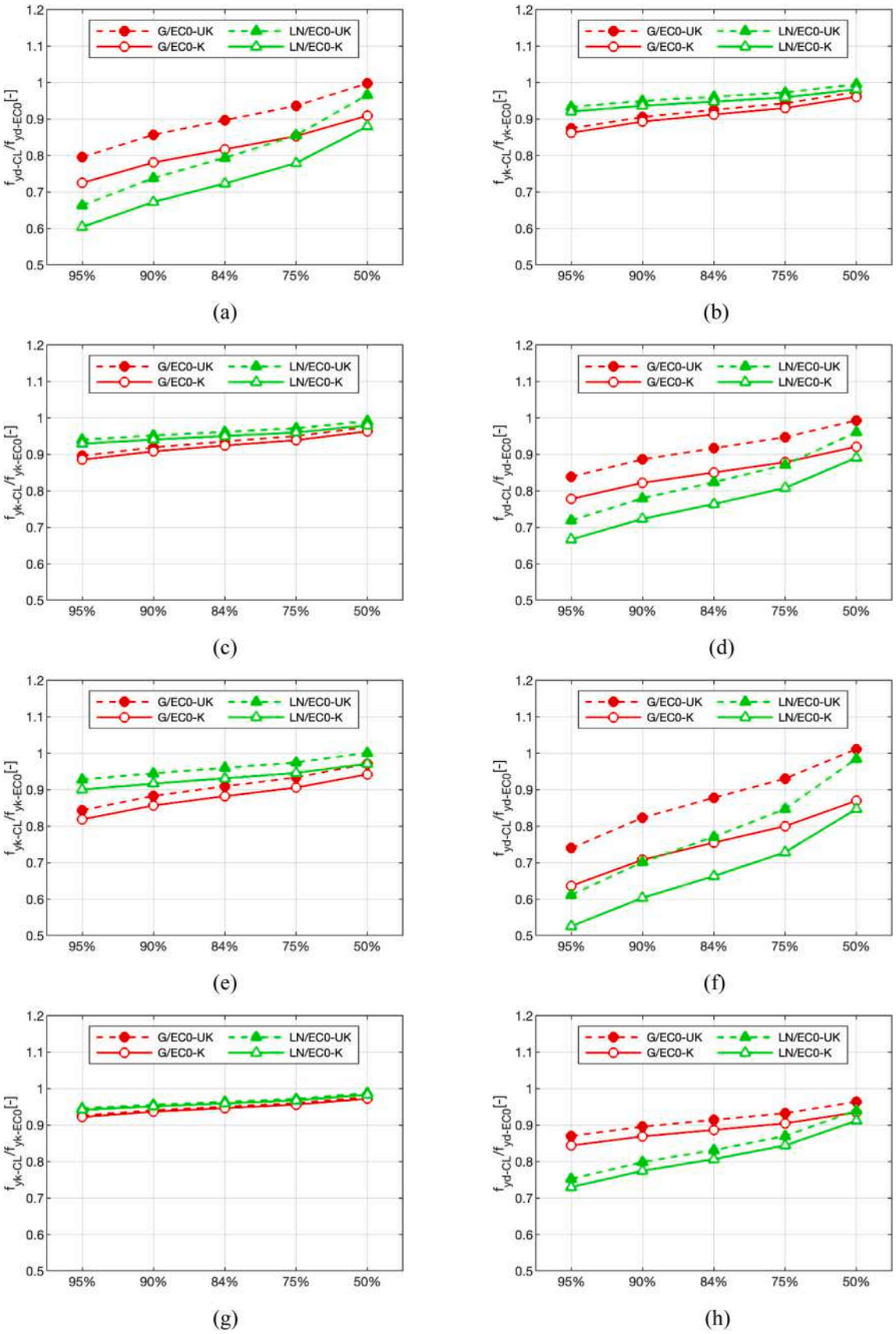

Fig. A5. Graphs showing the ratios between CL (at the different CI amplitudes) and EC0 yield strengths for both characteristic and ULS design values, considering both known and unknown COV: (a)-(b) dot-0, (c)-(d) dot-10, (e)-(f) dot-45, (g)-(h) dot-0&10.

.

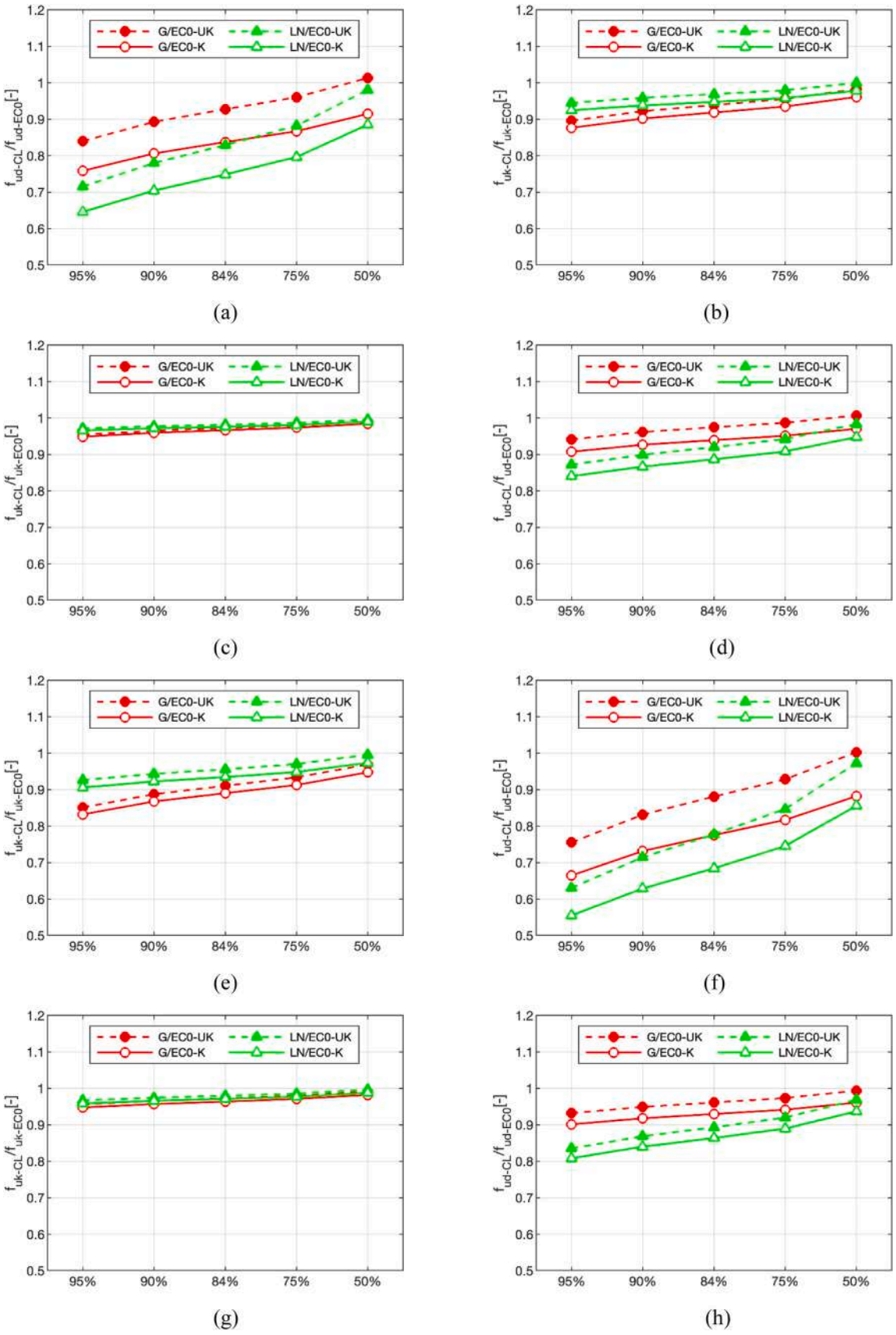

Fig. A6. Graphs showing the ratios between CL (at the different CI amplitudes) and EC0 ultimate strengths for both characteristic and ULS design values, considering both known and unknown COV: (a)-(b) dot-0, (c)-(d) dot-10, (e)-(f) dot-45, (g)-(h) dot-0&10.

.

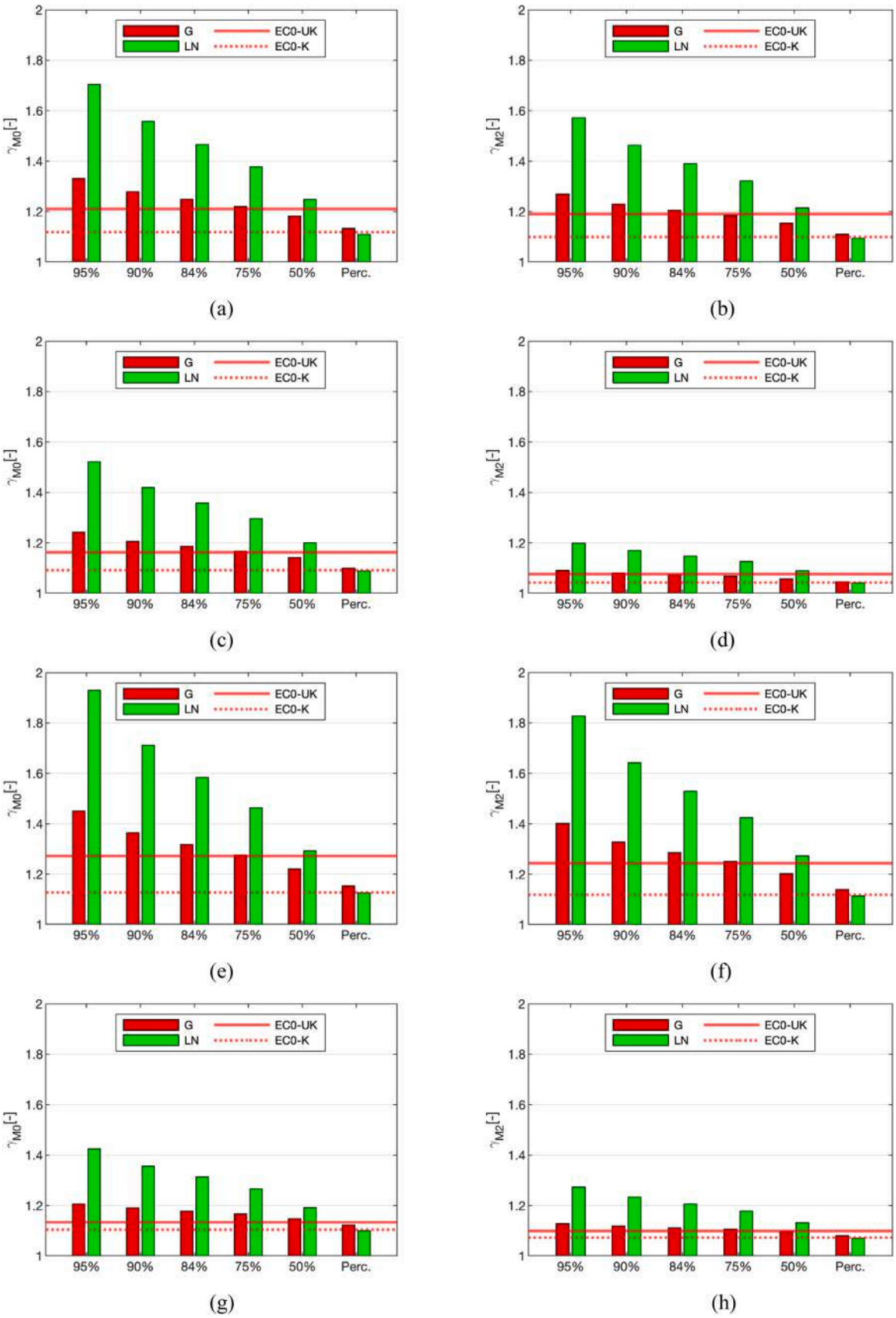

Fig. A7. Bar charts representing the material partial factors according to CL approach (for the different CI amplitudes), EC0 approach and the percentiles: (a) dot-0 (γ_{M0}), (b) dot-0 (γ_{M2}), (c) dot-10 (γ_{M0}), (d) dot-10 (γ_{M2}), (e) dot-45 (γ_{M0}), (f) dot-45 (γ_{M2}), (g) dot-0&10 (γ_{M0}), (h) dot-0&10 (γ_{M2}).

.

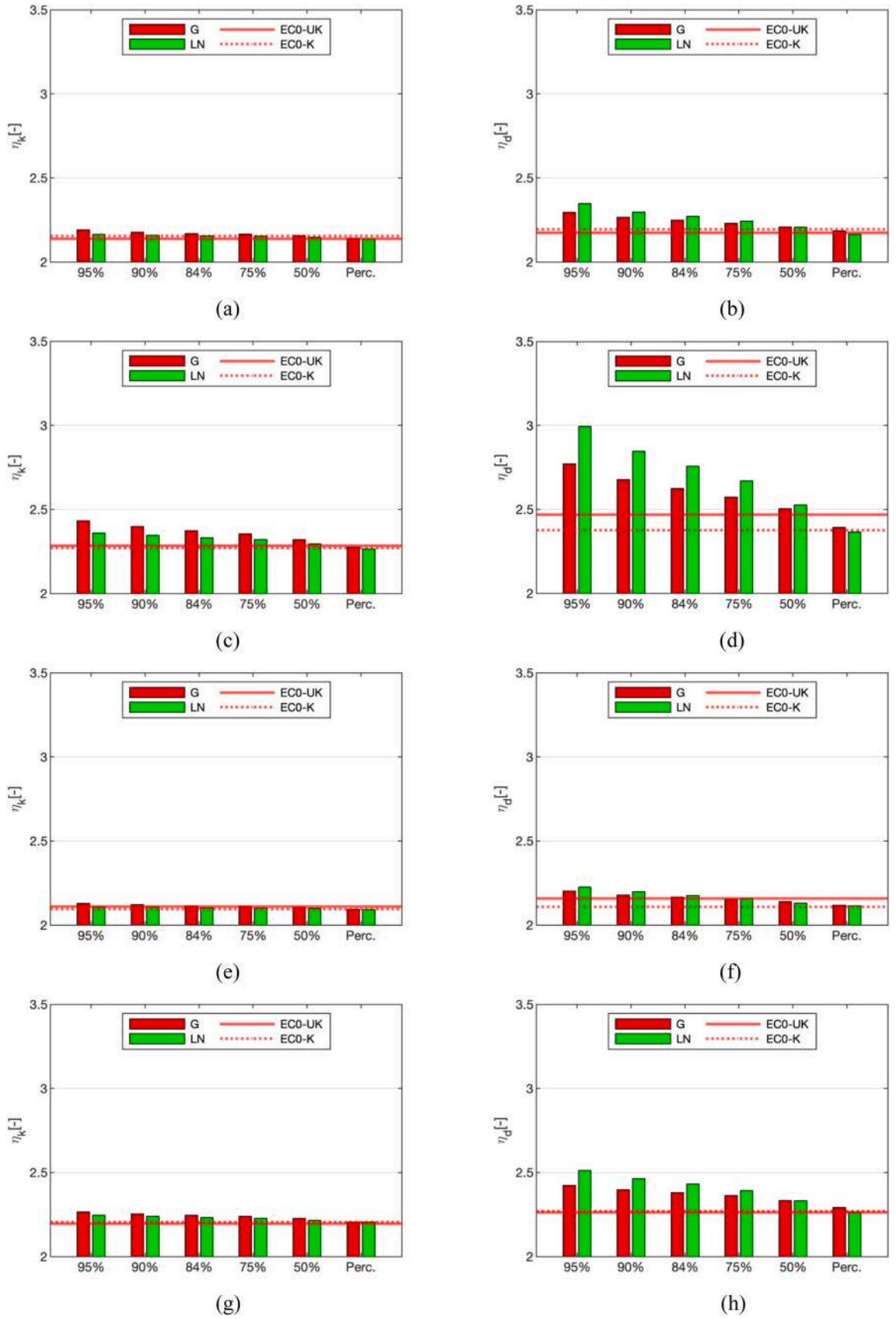

Fig. A8. Bar charts representing the strength hardening ratios according to CL and EC0 approaches and the percentiles: (a) dot-0 (η_k), (b) dot-0 (η_d), (c) dot-10 (η_k), (d) dot-10 (η_d), (e) dot-45 (η_k), (f) dot-45 (η_d), (g) dot-0&10 (η_k), (h) dot-0&10 (η_d).

.

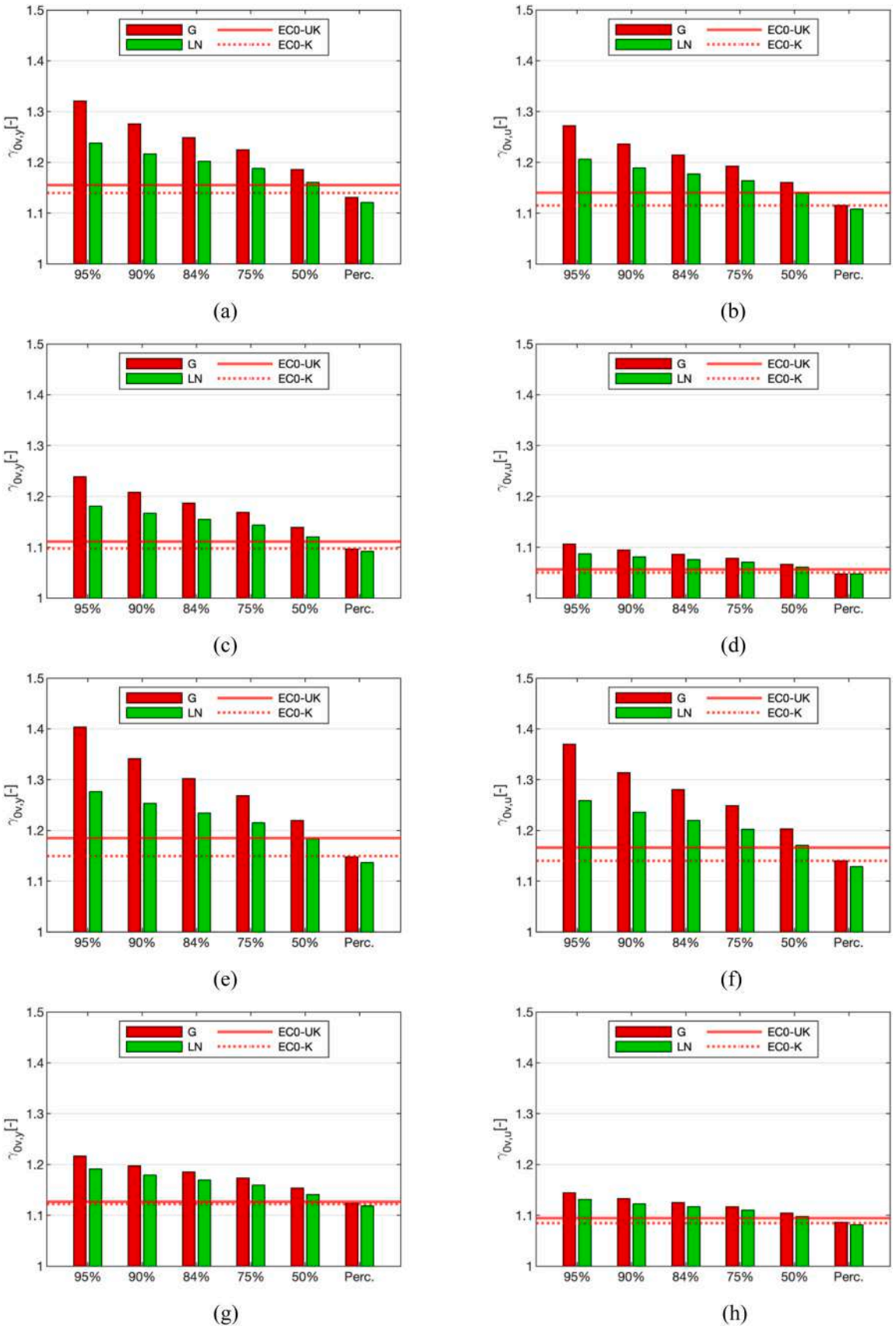

Fig. A9. Bar charts representing the material overstrength factors (γ_{0V}) according to CL approach (for the different CI amplitudes), EC0 approach and the percentiles: (a) dot-0 ($\gamma_{0V,y}$), (b) dot-0 ($\gamma_{0V,u}$), (c) dot-10 ($\gamma_{0V,y}$), (d) dot-10 ($\gamma_{0V,u}$), (e) dot-45 ($\gamma_{0V,y}$), (f) dot-45 ($\gamma_{0V,u}$), (g) dot-0&10 ($\gamma_{0V,y}$), (h) dot-0&10 ($\gamma_{0V,u}$).

.

References

[1] Wu P, Wang J, Wang X. A critical review of the use of 3-D printing in the construction industry. Autom Constr 2016;68:21–31.
[2] Boje C, Guerriero A, Kubicki S, Rezgui Y. Towards a semantic construction digital twin: directions for future research. Autom Constr 2020;114:103179.
[3] Kanyilmaz A, Demir AG, Chierici M, Berto F, Gardner L, Kandukuri SY, et al. Role of metal 3D printing to increase quality and resource-efficiency in the construction sector. Addit Manuf 2022;50. https://doi.org/10.1016/j.addma.2021.102541.
[4] Ye J, Kyvelou P, Gilardi F, Lu H, Gilbert M, Gardner L. An end-to-end framework for the additive manufacture of optimized tubular structures. IEEE Access 2021;9:165476–89.
[5] Shah IH, Hadjipantelis N, Walter L, Myers RJ, Gardner L. Environmental life cycle assessment of wire arc additively manufactured steel structural components. J Clean Prod 2023;389:136071. https://doi.org/10.1016/J.JCLEPRO.2023.136071.
[6] Laghi V, Gasparini G. Explorations of efficient design solutions for Wire-and-Arc Additive manufacturing in construction. Structures 2023;56:104883. https://doi.org/10.1016/J.ISTRUC.2023.104883.
[7] K. Tischner, S. Rappl, F. Riegger, A. Strasser, K. Osterminski, T. Kraenkel et al. , Bond Behavior of WAAM Reinforcements in Comparison to Conventional Steel Reinforcements, (2023). https://doi.org/10.3390/constrmater3020014.
[8] Silvestru V-A, Ariza I, Vienne J, Michel L, Aguilar Sanchez AM, Angst U, et al. Performance under tensile loading of point-by-point wire and arc additively manufactured steel bars for structural components. Mater Des 2021;205:109740. https://doi.org/10.1016/j.matdes.2021.109740.
[9] Dörrie R., Laghi V., Arrè L., Kienbaum G., Babovic N., Hack N., et al., Combined Additive Manufacturing Techniques for Adaptive Coastline Protection Structures, Buildings 2022, Vol. 12, Page 1806 12 (2022) 1806. https://doi.org/10.3390/BUILDINGS12111806.
[10] Laghi V, Palermo M, Gasparini G, Trombetti T. Computational design and manufacturing of a half-scaled 3D-printed stainless steel diagrid column. Addit Manuf 2020;36. https://doi.org/10.1016/j.addma.2020.101505.
[11] Laghi V, Palermo M, Gasparini G, Girelli VA, Trombetti T. On the influence of the geometrical irregularities in the mechanical response of Wire-and-Arc additively manufactured planar elements. J Constr Steel Res 2021;178:106490. https://doi.org/10.1016/j.jcsr.2020.106490.
[12] Laghi V, Palermo M, Tonelli L, Gasparini G, Ceschini L, Trombetti T. Tensile properties and microstructural features of 304L austenitic stainless steel produced by wire-and-arc additive manufacturing. Int J Adv Manuf Technol 2020:3693–705. https://doi.org/10.1007/s00170-019-04868-8.
[13] Hadjipantelis N, Weber B, Gardner L. Characterisation of the anisotropic response of wire and arc additively manufactured stainless steel. Ce/Pap 2021;4:1757–66.
[14] Laghi V, Tonelli L, Palermo M, Bruggi M, Sola R, Ceschini L, et al. Experimentally-validated orthotropic elastic model for wire-and-arc additively manufactured stainless steel. Addit Manuf 2021;42:101999. https://doi.org/10.1016/j.addma.2021.101999.
[15] Dinovitzer M, Chen X, Laliberte J, Huang X, Frei H. Effect of wire and arc additive manufacturing (WAAM) process parameters on bead geometry and microstructure. Addit Manuf 2019;26:138–46. https://doi.org/10.1016/j.addma.2018.12.013.
[16] Okita T, Kawabata T, Murayama H, Nishino N, Aichi M. A new concept of digital twin of artifact systems: synthesizing monitoring/inspections, physical/numerical models, and social system models. Procedia CIRP 2019;79:667–72. https://doi.org/10.1016/j.procir.2019.02.048.
[17] Gardner L, Kyvelou P, Herbert G, Buchanan C. Testing and initial verification of the world's first metal 3D printed bridge. J Constr Steel Res 2020;172. https://doi.org/10.1016/j.jcsr.2020.106233.
[18] Buchanan C, Gardner L. Metal 3D printing in construction: a review of methods, research, applications, opportunities and challenges. Eng Struct 2019;180:332–48. https://doi.org/10.1016/j.engstruct.2018.11.045.
[19] CEN), EN 1990: Eurocode 0 - Basis of Structural Design, (2002).
[20] Simões da Silva L, Tankova T, Marques L. On the safety of the European stability design rules for steel members. Structures 2016;8:157–69. https://doi.org/10.1016/j.istruc.2016.07.004.
[21] Kövesdi B, Somodi B. Comparison of safety factor evaluation methods for flexural buckling of HSS welded box section columns. Structures 2018;15:43–55. https://doi.org/10.1016/j.istruc.2018.05.006.
[22] Melhem MM, Caprani CC, Stewart MG. Reliability updating of partial factors for empirical codes: application to Super-T PSC girders designs at the ultimate limit state in bending. Structures 2022;35:233–42. https://doi.org/10.1016/j.istruc.2021.11.008.
[23] Monti G., Petrone, F., Test-Based Calibration of Safety Factors for Capacity Models, (2016). https://doi.org/10.1061/(ASCE)ST.1943.
[24] Laghi V, Palermo M, Gasparini G, Veljkovic M, Trombetti T. Assessment of design mechanical parameters and partial safety factors for Wire-and-Arc additive manufactured stainless steel. Eng Struct 2020;225. https://doi.org/10.1016/j.engstruct.2020.111314.
[25] Arrayago I, Rasmussen KJR, Real E. Statistical analysis of the material, geometrical and imperfection characteristics of structural stainless steels and members. J Constr Steel Res 2020;175. https://doi.org/10.1016/j.jcsr.2020.106378.
[26] Meza FJ, Baddoo N, Gardner L. Derivation of stainless steel material factors for European and U.S. design standards. J Constr Steel Res 2024;213. https://doi.org/10.1016/j.jcsr.2023.108383.
[27] Laghi V, Palermo M, Gasparini G, Girelli VA, Trombetti T. Experimental results for structural design of Wire-and-Arc additive manufactured stainless steel members. J Constr Steel Res 2020;167. https://doi.org/10.1016/j.jcsr.2019.105858.
[28] Kyvelou P, Slack H, Daskalaki Mountanou D, Wadee MA, Britton TBen, Buchanan C, et al. Mechanical and microstructural testing of wire and arc additively manufactured sheet material. Mater Des 2020;192:108675. https://doi.org/10.1016/j.matdes.2020.108675.
[29] Laghi V, Palermo M, Tonelli L, Gasparini G, Girelli VA, Ceschini L, et al. Mechanical response of dot-by-dot wire-and-arc additively manufactured 304L stainless steel bars under tensile loading. Constr Build Mater 2022;318:125925.
[30] Walker AM. A note on the asymptotic distribution of sample quantiles. J R Stat Soc Ser B (Methodol 1968;30:570–5. https://doi.org/10.1111/j.2517-6161.1968.tb00757.x.
[31] Meeker WQ, Han GJ, Escobar LA. Statistical intervals: a guide for practitioners and researchers. John Wiley & Sons; 2017.
[32] Laghi V, Girelli VA, Gasparini G, Trombetti T, Palermo M. Investigation on the elastic flexural stiffness of dot-by-dot wire-and-arc additively manufactured stainless steel bars. Eng Struct 2024;306:117680. https://doi.org/10.1016/J.ENGSTRUCT.2024.117680.
[33] Laghi V, Gasparini G, Trombetti T, Palermo M. Experimentally-validated buckling behavior of Wire-and-Arc additively manufactured stainless steel bars. Eng Struct 2024.
[34] MX3D Webpage, (n.d). www.mx3d.com.
[35] Oerlikon, (n.d). https://www.oerlikon.com/en/.
[36] Laghi V, Palermo M, Gasparini G, Girelli VA, Trombetti T. On the influence of the geometrical irregularities in the mechanical response of Wire-and-Arc Additively Manufactured planar elements. J Constr Steel Res 2021;178:106490. https://doi.org/10.1016/j.jcsr.2020.106490.
[37] Ramberg W., Osgood W.R., Description of stress-strain curves by three parameters, (1943).
[38] Rasmussen KJR. Full-range stress-strain curves for stainless steel alloys. Res Rep - Univ Syd, Dep Civ Eng 2001;59:1–44.
[39] Gardner L, Ashraf M. Structural design for non-linear metallic materials. Eng Struct 2006;28:926–34. https://doi.org/10.1016/j.engstruct.2005.11.001.
[40] Melchers RE, Beck AT. Structural reliability analysis and prediction. John wiley & sons; 2018.
[41] Massey FJJr. The Kolmogorov-Smirnov test for goodness of fit. J Am Stat Assoc 1951;46:68–78. https://doi.org/10.1080/01621459.1951.10500769.
[42] Sugiura N. Further analysis of the data by Akaike's information criterion and the finite corrections. Commun Stat Theory Methods 1978;7:13–26. https://doi.org/10.1080/03610927808827599.
[43] Khademi A. Statistical Intervals: A Guide for Practitioners and Researchers (2nd Edition). Journal of Statistical Software, 84. Book Reviews; 2018. p. 1–4. https://doi.org/10.18637/jss.v084.b01.
[44] Huang C, Kyvelou P, Gardner L. Stress-strain curves for wire arc additively manufactured steels. Eng Struct 2023;279:115628. https://doi.org/10.1016/J.ENGSTRUCT.2023.115628.
[45] Meza FJ, Baddoo N, Gardner L. Derivation of stainless steel material factors for European and U.S. design standards. J Constr Steel Res 2024;213. https://doi.org/10.1016/j.jcsr.2023.108383.